Organic vapors from Savannah and European Boreal fire emissions: Insights from photochemical and dark aging experiments in a smog chamber

Deeksha Shukla[1,a], Lejish Vettikkat[2], Mika Ihalainen[3], Markus Somero[3], Hendryk Czech*[1], Siegfried Schobesberger[2], Angela Buchholz[2], Iida Pullinen[2], Kerneels Jaars[4], Kajar Köster[3], Viet Le[5], Pasi Yli-Pirilä[3], Stefan J. Siebert[7], Pieter G. van Zyl[4], Annele Virtanen[2], Ville Vakkari[4,5], Olli Sippula[3,6], Ralf Zimmermann[1]

[1]Chair of Analytical Chemistry, University of Rostock, Germany
[2]Department of Technical Physics, University of Eastern Finland, Kuopio, Finland
[3]Department of Environmental and Biological Sciences, University of Eastern Finland, Kuopio, Finland
[4]Atmospheric Chemistry Research Group, Chemical Resource Beneficiation, North-West University, Potchefstroom, South Africa
[5]Finnish Meteorological Institute, Helsinki, Finland
[6]Department of Chemistry and Sustainable Technology, University of Eastern Finland, Joensuu, Finland
[7]Unit for Environmental Sciences and Management, North-West University, Potchefstroom, South Africa
[a]currently at: Aerosol Chemistry Department, Max Planck Institute for Chemistry, Mainz, Germany

Correspondence to: Hendryk Czech (hendryk.czech@uni-rostock.de)

Abstract

Biomass burning (BB) emits large amounts of pollutants in the particle and gas phases, with significant implications for air quality, human health and climate. Here, we investigate the emission of organic vapors from controlled burns of relatively understudied biomass fuels: woody plants and grasses from African savannah and European boreal forest surface using a high-resolution proton transfer reaction-mass spectrometer. To understand the effect of different oxidation regimes, organic vapors were aged in a 29 m^3 Teflon chamber, where photochemical and dark aging were simulated. The average total primary emission factors (EFs) for organic vapors varied considerably with fuel type, ranging from 69 to 161 g kg^{-1}. Photochemical aging led to substantial depletion of furanics, phenolics and oxygenated aromatics, accompanied by enhancements of carbonyl B compounds and O-containing compounds C<6 across experiments. In contrast, dark aging under low-NO_x conditions produced minimal compositional changes. Hierarchical clustering of relative composition showed clear regime dependence, with regime-associated differences accounting for 73% of the variance in group-level composition. Toluene and furan showed a strong negative correlation with secondary oxygenated volatile organic compounds (OVOCs), including anhydrides and small acids, consistent with their role as precursors. After 0.5 equivalent day of photochemical aging, organic vapors shifted to higher O/C (>0.70) and an increased fraction of $C_xH_yO_z$ ($z \geq 3$). These results highlight the integral role of OH·-driven photo-oxidation in governing the atmospheric evolution and composition of BB organic vapors and underscore the need for secondary organic aerosols (SOA) models to include non-traditional precursors.

Formatted: Font: 14 pt

Formatted: Font: 10 pt

Formatted: Font: 10 pt

1 Introduction

Formatted: Font: 12 pt

Biomass burning (BB), including forest and savannah fires, is a major source of atmospheric aerosols and trace gases in the atmosphere (Andreae, 2019) and is considered the second largest global source of organic vapors (Akagi et al., 2011; Yokelson, et al., 2008). BB emissions not only have significant impacts at local or regional scales but also may affect global atmospheric chemistry (Lewis et al., 2013) and Earth's climate (Keywood et al., 2013; Stocker et al., 2021). Organic vapors from BB emissions contain many oxygenated compounds and undergo further oxidation in the atmosphere, producing a mixture of products spanning a broad range of volatility (Koss et al., 2018)Low-volatile oxidation products partition into the condensed phase, form secondary organic aerosols (SOA) and may enhance cloud condensation nuclei (CCN) activity (Calvert et al., 2002; Kroll and Seinfeld, 2008; Pospisilova et al., 2020). Furthermore, the large amounts of NO_x and reactive organic vapors co-emitted from BB have the potential to form tropospheric O_3, which can be transported over large distances (Jaffe & Wigder, 2012; McKeen et al., 2002; Pfister et al., 2008; Vakkari et al., 2020). Emission of these organic vapors from BB varies significantly depending on factors such as biomass fuel, combustion conditions, fuel-moisture content, burning phase, time of the day and other variables (Chen et al., 2010; Czech et al., 2017; Rivera-Adorno et al., 2025; Sekimoto et al., 2018; Vakkari et al., 2018). Global warming has increased the frequency, intensity and behavior of wildfires in recent decades, making wildfires an important source of atmospheric pollution over time (Rogers et al., 2020). Recent evidence shows over twofold increase in frequency and magnitude of extreme wildfire events, with the largest increases occurring in the carbon-rich boreal and temperate conifer forests of the Northern Hemisphere. The long-range transport of wildfires from northern boreal regions like Siberia is known to affect the radiative balance and aerosol composition in the sensitive ecosystem of the Arctic region (Calì Quaglia et al., 2022; Schneider et al., 2024). Moreover, long-range transport of wildfire emissions in Canada substantially decreased the air quality in metropolitan areas of the US East Coast (Kolden et al., 2024). These findings highlight the increasing importance of understanding emissions from boreal forest wildfires and their atmospheric impacts.

In recent years, wildfire activity has intensified in Europe, with the continent recording its second-largest burned area in 2022 (EU-JRC, 2023) and approximately 500,000 ha burnt in 2023 (San-Miguel-Ayanz et al., 2023), which was the largest individual wildfire ever mapped in Europe. The impacts and severity of wildfires are expected to grow in response to climate change (Whitman et al., 2019). To understand the impact of wildfire emissions better, BB emissions have been extensively investigated either by field experiments (Brito et al., 2014; Garofalo et al., 2019; Gkatzelis et al., 2024; Hobbs et al., 2003; Liang et al., 2022a; Vakkari et al., 2014; Warneke et al., 2023) ~~and/~~or by simulating natural fire in a laboratory (Ahern et al., 2019; Akherati et al., 2020; Fang et al., 2021; Gilman et al., 2015). However, fewer studies (Hobbs et al., 2003; Sinha et al., 2003; Swap et al., 2003) exist related to savannah fire emissions and their aging, despite savannah fires accounting for nearly half of global fire-derived carbon emissions (van der Werf et al., 2017; van Wees et al., 2022). ~~their significant contribution to the global aerosol burden.~~ Boreal BB emissions are ~~,~~ acknowledged as a crucial contributor to Arctic climate change (Zhong et al., 2024). ~~,~~ North American boreal forests have been studied more extensively (Boby et al., 2010; Zhao et al., 2021), partly because of their greater extent and the prevalence of high-intensity crown fires. In contrast, European boreal forests, which are dominated by lower-intensity surface fires, remain comparatively understudied (Köster et al., 2024).~~.~~ Since boreal forests form a continuous circumpolar belt from Scandinavia across European Russia to

Siberia, results from Finnish biomass-burning emissions are also relevant for eastern high latitudes as a representation of the boreal fire regime, although there can be regional differences in fuel moisture and fuel/stand composition expected along an eastward gradient. ~~are rarely explored in European boreal forest surface fires compared to North American boreal forest (Boby et al., 2010; Zhao et al., 2021).~~

The atmospheric evolution of the BB plume is a complex process ~~and is~~ governed ~~affected~~ by several interacting processes including gas-phase oxidation, heterogeneous chemistry, evaporation and condensation of semi-volatile compounds, and plume dilution. ~~various factors like heterogenous chemistry and plume dilution.~~ Functionalization and ~~or~~ oligomerization reactions produce low volatility gas-phase species that gradually condense to form SOA; however, continued oxidation promotes fragmentation reactions, resulting in lower SOA yields (Kroll et al., 2009; Lambe et al., 2012). Plume-dilution can cause condensed semi-volatile compounds to evaporate, reducing the organic loading (Pagonis et al., 2023; Palm et al., 2020). ~~makes fragmentation reactions dominate resulting in lower SOA yields (Kroll et al., 2009; Lambe et al., 2012). Plume-dilution can cause condensed semi-volatile compounds to evaporate, reducing the organic loading (Pagonis et al., 2023; Palm et al., 2020).~~ These evaporated compounds may recondense after further oxidation, continuously altering the composition and properties of organic vapors (Akagi et al., 2012; Garofalo et al., 2019; Mason et al., 2001). The co-existence of primary emission and secondary formation products adds complexity to the evolution, making characterization of organic vapors critical. There exists a discrepancy between ambient wildfire plumes and those aged in laboratory smog chambers with respect ~~when it comes~~ to net SOA ~~secondary organic aerosol (OA)~~ formation with aging, smog chamber studies generally indicating stronger SOA formation (Hodshire et al., 2019). This discrepancy may partly arise from rapid atmospheric oxidation of ambient BB plumes, which promotes the early formation of BB-derived SOA and makes it increasingly difficult to distinguish between primary organic aerosol (POA) and SOA.

Formatted: Font color: Auto, English (United Kingdom)

Over the past decades, field and chamber studies have investigated the oxidation of BB emissions during either daytime, driven by OH·, or nighttime, driven by NO_3· and O_3 (Czech et al., 2024; Georgopoulou et al., 2025; Hodshire et al., 2019; Kodros et al., 2020; Tkacik et al., 2017; Yazdani et al., 2023). However, NO_3· chemistry can also be relevant during daytime due to suppressed photolysis in optically thick plumes (Decker et al., 2021). These atmospheric aging processes are likely to substantially alter the key properties of BB emissions with respect to climate and health. As BB plumes age, rapid oxidation of non-methane hydrocarbons (NMHCs) produces a complex mixture of oxygenated volatile organic compounds (OVOCs). Since the atmospheric oxidizing capacity is largely controlled by OH·, and OVOC photolysis is a major OH· source (Wolfe et al., 2022), OVOCs exert significant impacts on tropospheric photochemistry (Dai et al., 2025). Simultaneously, several OVOCs, particularly carbonyls, pose a threat to human health and have been associated with cytotoxic, mutagenic, and carcinogenic effects (Marques et al., 2021; Stabbert et al., 2017). Furthermore, the role of VOCs (Ahern et al., 2019; Akherati et al., 2020) and more recently, of semi-volatile or intermediate-volatility organic compounds (S/IVOCs) as key gas-phase precursors in SOA formation has been extensively investigated. A recent study (Li et al., 2024a) reported that IVOCs accounted for ~70% of the total SOA, more than twice the contribution from VOCs, providing the first direct evidence on their central role and advancing our understanding of the chemical drivers of SOA formation. However, the chemical complexity of organic vapors from BB emissions, along with analytical limitations, continues to pose challenges for detailed identification and quantification of a diverse range of species. As a result, there remains a limited understanding of major organic vapors from BB emissions, their

evolution and the effects of atmospheric aging on them. Furthermore, since BB emissions are ensembles of complex organic compounds, their collective reactivity often differs from that of individual species. This makes it important to investigate their behavior through bulk molecular-level characterization, which can offer valuable insights into their atmospheric dynamics.

Advancements in analytical instrumentation have significantly improved our ability to characterize the molecular-level composition of organic vapors. Traditionally, gas chromatography (GC) and multidimensional GC coupled with mass spectrometry (GC-MS) have been widely used to measure selected VOCs and NMHCs (Lewis et al., 2000). While these offline analytical techniques remain indispensable for analyzing specific compounds, they are limited by their focus on a narrower subset of analytes, extensive sample preparation/analyses times and potential for artifacts. Proton-transfer-reaction mass spectrometry (PTR-MS) emerged as a sophisticated technique for real-time detection of a broad range of volatile compounds with high sensitivity without pre-concentration or separation (Hansel et al., 1995; Yuan et al., 2017a). Subsequent integration with high-resolution time-of-flight analyzers (PTR-TOF-MS) expanded its analytical ability with higher mass-resolution and response time, thereby enabling the detection of lower-volatility compounds and highly oxygenated species (Bruns et al., 2017; Koss et al., 2018). High resolving power TOF-MS allows separation of compounds that are isobaric at unit mass resolution and enables molecular formula assignment, however, without an additional separation dimension (e.g. retention time), it cannot distinguish isomers that share the same chemical formula (Hatch et al., 2017). One option to improve the selectivity of PTR(-TOF)-MS analyses is to switch between different reagent ions (H_3O^+, NH_4^+, NO^+, O_2^+), which enhances sensitivity towards different compound classes (Reinecke et al., 2023), although in practice such switching must be sufficiently fast to capture rapid change in emissions, so hyper-fast GC (Gehm et al., 2021) offers an alternative route to separate and track dynamic changes in emissions while maintaining a reasonable time resolution. More recently, Vocus PTR-TOF-MS has introduced several technical innovations over earlier-generation PTR systems, most notably a redesigned chemical ionization source that substantially enhances ion transmission efficiency, resulting in higher detection of product ions (Krechmer et al., 2018). This advancement has expanded its detection capabilities for a wider range of VOCs, IVOCs and their oxidation products, such as monoterpene oxidation products with up to six oxygen atoms (Li et al., 2020)

In this study, we use a Vocus PTR-TOF-MS to elucidate how different oxidation regimes affect the emission of organic vapors from three globally relevant, yet relatively under-studied biomass fuels i.e. European boreal forest surface samples collected in Finland, and woody plants and grasses sourced from a grassland savannah environment in South Africa. We begin by discussing the characteristics of primary organic vapor emissions for each biomass fuel. We then examine how these organic vapors evolve and how their chemical composition transforms under simulated photochemical and dark aging in a smog chamber to highlight the atmospheric relevance of the results. High-resolution, real-time measurements of organic vapors from such understudied biomass sources are essential for advancing our current understanding of BB contributions to the global aerosol burden and associated environmental and climate impacts.

2 Material and methods

2.1 Fuels and bBiomass-burning (BB) experiments

The experiments were conducted under the framework of the boreal and savannah fire aerosol aging (BASFAA) campaign that took place at the ILMARI facility in the University of Eastern Finland, Kuopio, Finland, during May-June 2022. Laboratory burns of three different biomass fuels, i.e. boreal forest surface from Finland, woody and

Formatted: Font: 12 pt

Formatted: Font: 11 pt

Formatted: Normal

grassy material from the savannah in South Africa, were performed. European boreal forest surface samples (including vegetation, litter and soil organic horizon) were collected from the Evo experimental fire area (Köster et al., 2024), located in an even-aged 75-year-old Scots pine stand, while woody plants and grasses were collected from a grassland savannah environment near the Welgegund atmospheric measurement station (Jaars et al., 2016) in South Africa. The moisture content was analysed at an accredited laboratory (Eurofins Environment Testing Finland Oy) and was 9.4% for savannah wood, 8.6% for savannah grass and 9.6% for the boreal forest surface, representing dry conditions. More detailed information on the biomass samples is provided in the Table S1. ~~-~~Further details of each biomass, including their elemental composition ~~moisture, carbon content~~ etc., are documented in a previous publication focused on primary emission characterization (Vakkari et al., 2026).~~(Vakkari et al., 2025).~~

Combustion was conducted under an open-stack setup designed to mimic natural burning and dilution conditions, following the approach by (Christian et al., 2003), but on a smaller scale. The fuel bed had a diameter of approximately 50 cm. A 6 cm diameter sample holder was used for savannah biomasses, whereas a 23 cm diameter sample holder was used for the boreal forest surface to accommodate larger fuel load. ~~with fuel bed diameter of approx. 50 cm where a 6 cm in diameter sample holder was placed for the savannah biomasses. For boreal forest surface the sample holder was 23 cm in diameter.~~ Combustion was conducted as batch burns where a pre-weighed fuel load ~~(~~typically 50-60 g for savannah fuels and ~500 g of boreal forest surface was placed on the fuel bed and ignited using a resistor heating element. Before each experiment, a continuous flow of zero air (Adco Instruments Inc., Model 737-250), was used to flush the smog chamber and sampling lines through lines to prevent cross-contamination between burns and to maintain a low VOC background. The sample was introduced from the stack into a 29 m^3 smog chamber (Leskinen et al., 2015) via a two-stage dilution-system comprising of a porous tube diluter followed by an ejector diluter (Dekati, Type, Finland). The smog chamber is a collapsible Teflon bag chamber equipped with 47 blacklight lamps (354 nm, Sylvania F40 W/350 BL) (Leskinen et al., 2015). The relative humidity inside the chamber was maintained at 20% for savannah grass and savannah wood experiments and 50% for boreal forest surface experiments to replicate characteristic daytime relative humidity conditions for each environment during active fire seasons, ~~-~~using a humidification setup described in Leskinen et al. (2015). The instrumentation layout at the ILMARI facility was similar to as described in (Tiitta et al., 2016)). A general schematic of the experimental setup is presented in Figure S1 in the Supplement. Detailed description of the experimental design and associated instrumentation are provided in (Vakkari et al., 2026)~~Vakkari et al. (2025)~~.

Details of the 21 experimental burns used in the organic vapor analysis (savannah grass, n=9; savannah wood, n=7; boreal forest surface, n= 4; blank experiment, n=1), including dilution factor, injected mass concentration (Primary OA, μg m^{-3}), primary rBC concentrations (μg m^{-3}), background subtracted CO_2 and CO concentration (ppm), and type of aging performed for each experiment are provided in Table S2. The median primary size distributions grouped according to MCE ranges, for each biomass fuels are presented in Figure S3. A blank experiment was conducted on 11 May 2022 following the same experimental procedure as the BB experiments, except that no biomass fuel was burned (Table S2). No measurable background signals were observed for the monitored gas species either before or after aging during the blank experiment.

Formatted: English (United States)

Formatted: List Paragraph, Right: -0.59 cm

2.2 Aging procedure in smog-chamber

After injection into the chamber and approximately 15 minutes of thorough mixing, a 45-minute period of primary measurements was made. After primary measurements, oxidant (O_3) was injected into the chamber, and aging experiments were conducted in both photochemical and dark conditions. In dark aging experiments, the aim was to represent remote wildfire plumes with little anthropogenic influence, and therefore no additional NOx was added. Additionally, no OH· scavenger was added and no OH· formation was observed as indicated by constant butanol concentration. Initial concentration of approximately 100 ppb of O_3 was injected. The elevated O_3 concentration was used to simulate a full night of atmospheric oxidation over a shorter experimental period. In photochemical aging experiments, O3 was injected to an initial concentration of 50 ppb to represent regional daytime background atmospheric conditions. Externally added O_3 (50 ppb) and H_2O_2 (0.5 mL of 30% v/v solution) in the presence of UV-lights resulted in the formation of OH·, thereby simulating realistic daytime atmospheric oxidation conditions in which multiple oxidants co-exist. The aging experiments continued for over 4.5 hours of wall-clock time after the oxidant injection was completed. Representative time series of one photochemical and one dark aging experiment for savannah grass biomass fuel are shown in the Figure S2 in the Supplement. ~~only O_3 was injected, while in photochemical aging experiments, along with O_3, UV-lights were switched on and additional H_2O_2 was added into the chamber to generate OH·. Initial O_3 concentration was approximately 50 ppb for photochemical aging experiments and 100 ppb for dark aging experiments.~~ The OH· exposure in the chamber was traced by injecting butanol-d9 and monitoring its decay during experiments (Barmet et al., 2012). A butanol-d9 reaction rate coefficient of $3.4x10^{-12}$ cm^3 $molecule^{-1}$ s^{-1} at 295 K was assumed (Allani et al, 2021). At the end of photochemical aging experiments, the final OH exposures ranged from 1.3×10^{11} to 2.6×10^{11} molecules cm^{-3} s. The extent of photochemical age is discussed in terms of equivalent (eqv.) day as 24 hours spent at the average ambient OH· concentration of $1.5x10^6$ molecules cm^{-3} (Cheung et al., 2025a; Mukherjee et al., 2025). In ~~the~~ dark aging experiments, NO_x concentrations in the chamber were low, and under these low-NO_x (<10 ppb) conditions, formation of NO_3· is expected to be limited, so dark aging was largely driven by O_3. The O_3 exposure was calculated by O_3 concentrations integrated over time, and at the end of dark aging experiments, the O_3 exposure ranged from 4.6×10^{16} to 5.3×10^{16} molecules cm^{-3} s. ~~then the A~~ambient O_3 concentration of $7x10^{11}$ molecule cm^{-3} (Ziemann and Atkinson, 2012) was used to convert the exposure into eqv. atmospheric day for dark aging experiments. OH· and O_3 concentration and exposure at the end of each photochemical and dark aging experiment are presented in Table S3 and S4 in the Supplement.

~~Details of the 21 experimental burns used in the organic vapor analysis (savannah grass, n=9; savannah wood, n=7; boreal forest surface, n= 4; blank experiment, n=1), including modified combustion efficiency (MCE), fuel type and aging condition are provided in supplementary information (Table S1).~~

For primary measurements, data were averaged over a 30-minute period before the addition of oxidant, and for aging experiments, averaged over the time interval corresponding to 0.5 eqv. day of atmospheric aging for all experiments, providing a standardized reference point for comparing photochemical and dark aging experiments conducted on different days under different oxidant exposures. In photochemical aging experiments, time-zero is referred to as the moment when UV lights were switched on, whereas in dark aging experiments, it's when O_3 was injected in the chamber.

2.3 Measurements and analysis of organic vapors

Formatted: Subscript
Formatted: Subscript
Formatted: Subscript
Formatted: Subscript
Formatted: Subscript
Formatted: Superscript
Formatted: Superscript
Formatted: Superscript
Formatted: Subscript
Formatted: Superscript
Formatted: Superscript
Formatted: Superscript
Formatted: Subscript
Formatted: Normal, Right: 0 cm, Tab stops: Not at 15.87 cm
Formatted: Font: 11 pt

The VOC measurements were conducted using a Vocus PTR-TOF-MS (Tofwerk AG, Aerodyne Research Inc; Krechmer et al., 2018) (hereinafter referred to as PTR-MS). VOCs with proton affinity greater than that of water are ionized by the primary ion H_3O^+ to form protonated VOC ions. Most VOCs can be detected using this technique. However, small alkanes, ethene and ethyne with low proton affinities remain undetected by PTR-MS. While the proton affinities of larger alkanes increase with molecular size (Fu et al., 2022), their ionization remains inefficient, and detection is compromised by extensive fragmentation (Gueneron etal., 2015). The proton transfer reaction for a VOC, V can be expressed as in Equation 1:

$$V + H_3O^+ \rightarrow VH^+ + H_2O \quad (1)$$

This PTR-MS has a focusing ionization molecule reactor (FIMR), which can focus the ions to the central axis, reducing the detection loss and thereby increasing the sensitivity. An additional advantage is that the water mixing ratio inside the FIMR is >15 % v/v, and hence there is no humidity dependence on the sensitivity. The drawback is that a quadrupole low-mass filter is used to reduce the primary ions reaching and degrading the MCP, hence normalization is not possible, and regular calibrations are needed. The transmission of *m/z* below 50 is also compromised.

The PTR technique is generally regarded as a soft ionization technique compared to electron impact ionization. However, the $[RH]^+$ ions generated (Equation 1) can fragment inside the reactor due to the added energy from the exothermic protonation reaction and collisions (Li et al., 2022a;Gueneron et al., 2015). Higher collision energy tends to suppress the water clustering of both reagent and product ions; however, it can also promote fragmentation of protonated ions (Li et al., 2022a). In this study, PTR-MS FIMR was operated at 2.5 mbar pressure, 100 °C temperature and an electric field strength of 57.5 V cm^{-1}, resulting in the field strength of 118.5 Townsend (10^{-17} V cm^2). These conditions were selected to achieve a balance so that excessive formation of water-cluster ions was avoided while maintaining stable protonated analyte ions with limited fragmentation. For α-pinene, the measured ion signals were distributed at *m/z* 81 (49%) and *m/z* 137 (51%), which was in line with a previous study (Simon et al., 2023). Fragmentation however was not accounted for individual ions, therefore compound-dependent fragmentation may cause over- or underestimation of the mixing ratios for certain molecular ions.

The chamber air was sampled into the PTR-MS through a 3 m long polytetrafluoroethylene (PTFE) tubing (6mm O.D, 5mm I.D.) with an extra flow of 3 lpm. The PTR-MS was operated at 1 Hz and was averaged to a working time resolution of 10 seconds. The PTR-MS data were recorded in Hierarchical Data Format version 5 (HDF5) using software called TofDaqRec. These raw data files were analyzed using the MATLAB-based tofTools R612 (Junninen et al., 2010), where custom peak shape determination, mass calibration, resolution function determination, and high-resolution peak fitting were performed. The mass transmission function and the ratios of measured and calculated sensitivities for a series of ions were used for data-quantification and conversion of ion-counts to parts per billion by volume (ppbv). The PTR-MS during the campaign had a mass accuracy of <5ppm with a mass resolving power of ~10000 Th/Th, which enabled reliable separation of many isobaric ions and molecular formula assignment for the identified signals.~~h~~.

Regular automated single-point calibrations (n=80) were performed using a gas mix of 14 calibration standards (Apel Reimer Environmental Inc.). The compounds calibrated with the standards were ethanol, acetonitrile, acetone, acrylonitrile, isoprene, methyl vinyl ketone (MVK), methyl ethyl ketone (MEK), benzene, m-xylene, α-pinene, 1,2,4-trimethylbenzene, siloxanes (D4 and D5) and β-caryophyllene. The calibration gas contained approximately

1 ppmv (except for β-Caryophyllene at 100 ppbv) and was diluted with zero air from the zero-air generator (Tofwerk AG) to achieve a target mixing ratio of 4 ppbv for the single-point calibrations. Limits of detection (LODs) for the 14 calibrants were estimated from background measurements as the 3σ (at 10 s) and are presented in ~~supplementary information (~~Table S5~~2)~~. The maximum sensitivity was observed for acetone and was used as the sensitivity factor for calibrating all non-calibrant ions. Hence, the reported ppbv values represent lower limits. To calculate uncertainties in instrument precision, uncertainties in VOC calibration gas mixing ratio (5%) and in the MFCs used for dilution (1% each) were used. An uncertainty of 7.2% resulted for acetone. Thus, the uncertainty in the total VOC concentration from the PTR-MS is estimated to be 10%, in agreement with (Jensen et al., 2023). The instrument zeros were done regularly for 30 seconds every 15 minutes. The zeros were linearly interpolated and subtracted from the measured data.

All detected and identified ions (n=436) except the primary ions $(H_20)_nH^+$, and ions containing deuterated hydrogen (^2H), water clusters, silicon (Si) and fluorine (F) were used for further analysis. Approximately 61% of the total organic vapor mass measured using the PTR-MS was assigned. The compositional analysis and discussion presented in this study are based on this chemically assigned fraction of organic vapors.

2.4 Data processing and Quantification

MCE provides a measure of combustion characteristics that reflects the relative contributions of flaming and smoldering combustion and is defined as the ratio of CO_2 to sum of CO_2 and CO emissions (Ward & Radke, 1993; Akagi et al., 2011).Flaming combustion is typically associated with MCE values larger than 0.1, whereas smoldering combustion is associated with MCE values smaller than 0.9 (Akagi et al., 2011; Yokelson et al., 1999). MCE values between 0.8-0.9 represent a mix of flaming and smoldering combustion (Jen et al., 2019). In this study, MCE ~~as a function of time~~ was calculated as a function of time from primary ~~flue gas~~ CO_2 and CO concentrations following Akagi et al. (2011). The emission factors (EFs; g kg^{-1} dry fuel) of species *i* were calculated following a carbon mass balance approach (Yokelson et al., 1999) following the implementation described by Vakkari et al., 2026as shown in Equation 2; ~~as per Equation 2:~~

$$EF_i\left(\frac{g}{kg}\right) = F_c \times 1000 \times \frac{MW_i}{12} \times \frac{ER_i}{\sum_{i=1}^{n} \frac{\Delta C_j}{\Delta CO}} \quad (2)$$

~~$EF_i\left(\frac{g}{kg}\right) = F_c \times 1000 \times \frac{MW_i}{12} \times \frac{ER_i}{\sum_{j=1}^{n} \frac{C_j}{\Delta CO}}$~~

Here, EF_i refers to the mass (g) of species (*i*) emitted per unit mass (kg) of dry fuel burned, where *j* denotes the chemical species for which the EF (g kg^{-1} dry fuel) is being calculated. F*c* is the fuel carbon fraction, MW_i is the molecular weight of the species (*i*), and ER_i is the emission ratio of species (*i*) with respect to ΔCO. In the denominator, *j* denotes each carbon-containing species included in the carbon mass balance, and ΔC_j is the excess carbon concentration of species *j*. ~~, and C_j is the number of moles of carbon for species (j). In T~~the summation includes ~~,~~ carbon emitted as CO_2, CO, CH_4, VOCs, OC, and BC (Vakkari et al., 2026). ~~is included (Vakkari et al., 2025).~~Background concentrations measured before sample injection were subtracted for each species. Fc, measured at Eurofins Environment Testing Finland Oy according to DIN EN ISO 16948:2015-09 protocol was 48.8% for savannah wood, 43% for savannah grass, and 42.8% for boreal forest fuel, with a measurement uncertainty of 2%

Formatted: Right: 0 cm
Formatted: Font: (Default) Times New Roman, 10 pt, Bold
Formatted: Normal, Indent: Left: 0 cm
Formatted: Font: 11 pt
Formatted: Font color: Auto
Formatted: Font color: Auto
Formatted: Font color: Auto
Formatted: Font color: Auto
Formatted: Font color: Auto
Formatted: Font color: Auto
Formatted: Font color: Auto
Formatted: Font color: Auto
Formatted: Font color: Auto
Formatted: Font color: Auto
Formatted: Font color: Auto
Formatted: Font color: Auto
Formatted: Font color: Auto
Formatted: Font color: Auto
Formatted: Font color: Auto
Formatted: Font color: Auto
Formatted: Font color: Auto
Formatted: Font color: Auto
Formatted: Font color: Auto
Formatted: Font color: Auto
Formatted: Font: Italic
Formatted: Superscript
Formatted: Font: Italic
Formatted: Font: Italic
Formatted: Font: Italic
Formatted: Font: Italic

(Vakkari et al., 2026). ~~For each species, background concentration before sample injections has been subtracted. F_e was 48.8% for savannah wood, 43% for savannah grass and 42.8% for boreal forest fuel (Vakkari et al., 2025).~~ Outlier detection was performed using Hampel filter (median ± median absolute deviation) for each detected ion (Pearson et al., 2016), and at each time step, a robust z-score was computed as the absolute deviation from the local median divided by 1.4826×MAD. Points with a robust z-score larger than a threshold (k ≈ 5) were flagged as candidate spikes. Isolated spikes were removed only when they occurred as short excursions (<3 points); longer changes were retained as real variability. Only 0.28% of all measurements were identified as outliers. A total of 436 measured molecular ions were then classified according to their functional groups into 11 major classes (Table S~~6~~3) similar to previous combustion studies (Bhattu et al., 2019; Hartikainen et al., 2024; Wang et al., 2025). These classes include hydrocarbons (C_xH_y), aromatic hydrocarbons (ArHCs) including single ring aromatics and polycyclic aromatic hydrocarbons, oxygenated aromatic, furanic, O-containing compounds containing C<6 and C≥6, CHN and CHNO, phenolic and carbonyl compounds. Carbonyl compounds were classified into carbonyl A and carbonyl B by analyzing their emission trends during the photochemical aging experiments. For each compound, a robust Theil-Sen estimator was used to calculate the slope of its EF over the ageing period across biomass type. Compounds were assigned to carbonyl A class if they exhibited a negative slope (decreasing trend) in at least 80% of the experiments, whereas compounds exhibiting a positive slope (increasing trend) in at least 80% of the experiments were assigned to carbonyl B class. ~~Compounds with ≥80% experiments showing a negative slope (decreasing trend) were assigned to carbonyl A, while those with a positive slope (increasing trend) were assigned to carbonyl B.~~ The molecular formulas assigned to each compound class are provided in Table S~~6~~3 in ~~supplementary information~~the Supplement.

The degree of unsaturation of detected ions was estimated using double bond equivalents (DBE) which describes the total amount of double bond and ring structures in the molecule. DBE values were calculated as per Equation 3:

$$DBE = C - \frac{H}{2} + \frac{N}{2} + 1 \quad (3)$$

Here, C, H, N represent the number of carbons, hydrogen, and nitrogen present in the molecules, respectively. Mass defect plots for organic vapors were used further to visualize the difference in mean mixing ratio of compounds between fresh and aged emissions and to highlight dominant signals present for each fuel and aging condition. Compounds were further classified into elemental classes such as C_xH_y, $C_xH_yN_i$), C_xH_yO (z <3), $C_xH_yO_z$ (z ≥ 3), and $C_xH_yO_zN_i$ where *x, y, z* and *i* denote the numbers of carbon, hydrogen, oxygen and nitrogen atoms, respectively. Marker sizes were scaled to the relative mean mixing ratio within each class.

2.5 Statistical analysis

A cluster map (hierarchically clustered heatmap) was used to visualize relationships between samples and compound groups, using the SciPy library in Python 3.9. The cluster map shows group-level mean mixing ratios aggregated by compound group (rows) and oxidation regime-resolved samples (columns; date x fuel x regime). Group means were standardized by sample (column; z scored within each sample across groups), so the associated heatmap displays how many standard deviations a given compound group lies from that sample's mean, indicating relative enrichment/depletion of compound groups within each sample. Dendrograms obtained with Euclidean distances and Ward's minimum-variance algorithm (Nguyen et al., 2021) illustrate similarity among compound

Formatted: Font: (Default) Times New Roman, 10 pt
Formatted: Justified, Line spacing: 1.5 lines
Formatted: Font: (Default) Times New Roman, 10 pt
Formatted: Font: (Default) Times New Roman, 10 pt
Formatted: Font: 11 pt
Formatted: Font: (Default) Times New Roman, 10 pt, Font color: Black

groups and among samples (date x fuel x regime). MCE was included as a continuous annotation track to aid interpretation but was not used to compute clustering distances. Tree fidelity was assessed with the cophenetic correlation coefficient, which measures the agreement between dendrogram heights and the underlying distance matrix, and is interpreted similarly to Pearson's correlation coefficient (Sokal and Rohlf, 1962). Multivariate comparisons were performed in the same space used for the cluster map i.e. standardized sample x group matrix. One-way Permutational Multivariate Analysis of Variance (PERMANOVA) (Anderson, 2001, 2017). Euclidean distance matrices were used to quantify how much of the variance in composition was associated with regime (fresh, O_3, UV+O_3), fuel (savannah grass, savannah wood, boreal forest surface), and to test regime effects within each fuel. For each model, pseudo-F statistic, R^2 (proportion of variance explained), and p-value were obtained from 999 permutations of the sample labels.

To assess whether the differences in composition were related to MCE, a Mantel test (Spearman) was additionally performed between the Euclidean composition distance matrix and a distance matrix of pairwise |ΔMCE|, using 999 permutations to assess significance.

3 Results and Discussion

3.1 Primary gaseous organic emissions

A total of 436 ions were identified based on the elemental composition derived from MS and were then classified into 11 major classes using formula-based functional-group assignments. The average MCE during batch combustion were between 0.59 to 0.97. The EFs of organic vapors varied based upon the biomass fuel type and MCE values, and generally lower MCE values corresponded to higher EFs of organic vapors, excluding two glowing-phase experiments (MCE 0.8 or less) with low EFs values (Vakkari et al., 2026). ~~(Vakkari et al., 2025).~~ In this study, glowing phase experiments represent the phase after the flames had died down. Under low-MCE and low-temperature conditions, organic vapor emissions are likely dominated by primary pyrolysis products of biomass (Akagi et al., 2011). However, combustion under low-MCE conditions generally proceeds at a lower burn rate than flaming combustion. Thus, despite higher EFs, the mass of emitted pollutants after a certain time interval is typically larger for flaming combustion. The total EFs for the gaseous organic compounds had an average (standard deviation) value of 69 (21), 147 (53) and 161 (22) g kg^{-1} fuel burnt for savannah grass, savannah wood and boreal forest surface across all the experiments. The average total EFs for each fuel were relatively higher than the total average EFs reported from previous studies, however, the number of ions considered in this study was approximately 3–4 times higher than in previous studies (Gkatzelis et al., 2024; Koss et al., 2018; Permar et al., 2021; Travis et al., 2023). Figure 1 shows EFs for each of the classes in a box-and-whisker plot, highlighting the distributional behavior with median and interquartile ranges (IQR) reported for each fuel x class in the Supplement ~~supplementary information~~ (Table S74).

Formatted: Font: (Default) Times New Roman, 10 pt, Font color: Black

Formatted: Font: (Default) Times New Roman, 10 pt, Font color: Black

Formatted: Font: 12 pt

Formatted: Font: 11 pt

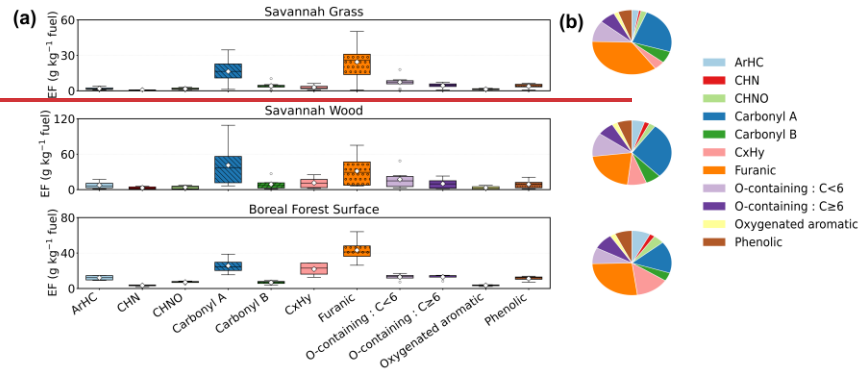

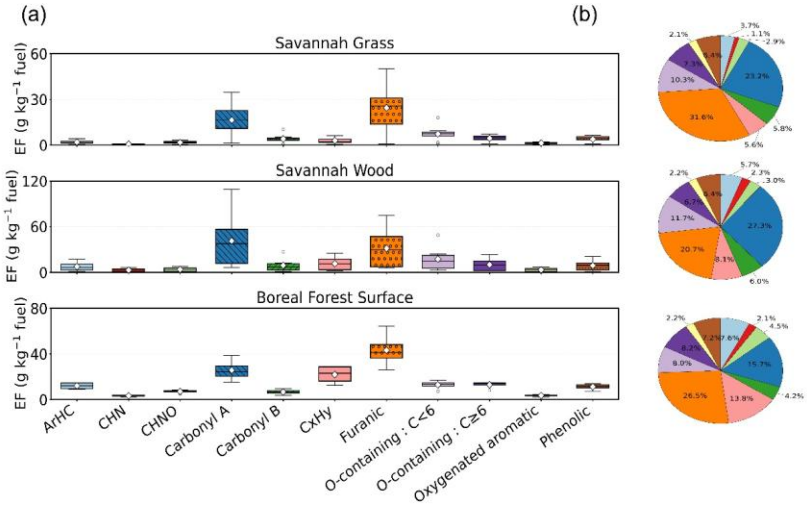

Figure 1. (a). Fresh emission factors (EFs) distributions by compound class for savannah grass, savannah wood, and boreal forest surface. For each fuel, boxplots show the variability across experiment days of class-averaged EFs (g kg^{-1} fuel). Boxes are colored by class (ArHC, CHN, CHNO, carbonyl A, carbonyl B, C_xH_y, furanic, O-cont.: C<6, O-cont.: C≥6, oxygenated aromatic, phenolic). Boxplots use 1.5×IQR (Interquartile Range) whiskers; hollow circles = outliers; white diamonds = mean. Note that different y-axis scales are used for the three biomass fuels. (b) Companion pie charts showing the mean fractional contribution (%) of each class to the total Fresh EF for the same biomass fuels.

Fresh emissions were dominated by small oxygenate species like furanic, carbonyl A and O-containing compounds with C<6. Savannah wood exhibited the most variable fresh EFs across the classes, with a median value of 37.4 g kg^{-1} fuel (IQR 56.2-11.7) for carbonyl A, which can be attributed to highest variability in MCE for savannah wood

experiments (0.59-0.95) compared to MCE ranges in savannah grass (0.76-0.97) and boreal forest surface (0.74-0.84) experiments. Savannah grass showed the lowest overall emissions with furanic compounds dominating the emissions with a median value of 25.7 g kg^{-1} fuel (IQR 30.9-13.8). The differences in emissions largely reflected variations in MCE across the biomass fuels. In particular, the glowing combustion cases for savannah grass contributed to its lower overall EFs.

Boreal forest surface biomass fuel showed high EFs of hydrocarbons (C_xH_y) with a median value of 23.0 g kg^{-1} fuel (28.7-16.2), which was 2-fold and 10-fold higher than the median C_xH_y from savannah wood and savannah grass, respectively. The relative contribution of individually measured chemical classes to the total EF is shown in Figure 1b. Carbonyl A and furanic compounds alone contributed to the major fractions of total primary emission, especially for savannah fuels (59% for savannah grass and 49% for savannah wood). Carbonyl compounds are key precursors for atmospheric organic acids and strongly facilitate the formation of SOA (Liu et al., 2022). They can be formed as intermediate gaseous oxidation products when certain VOCs react with atmospheric oxidants, and because some of these carbonyls are relatively water-soluble, they can dissolve into the aqueous aerosol phase and undergo further particle-phase reactions, e.g., oligomer formation of α-dicarbonyls (Kawamura et al., 2013). Furan and their derivatives, acknowledged as 'non-traditional SOA precursors', have been identified as predominant species in BB emissions and gained attention in recent years (Bruns et al., 2017; Hartikainen et al., 2018; Li et al., 2024b; Müller et al., 2016). A study by Coggon et al., 2019 also suggested furans as significant precursors of secondary organic vapors measured by PTR-TOF-MS and other chemical ionization mass spectrometers and shed light on the importance of furan chemistry in biomass burning plumes. In this study, OVOCs such as carbonyls, furanic, O-containing compounds, oxygenated aromatics and phenolic compounds form the major fraction of emissions, i.e. >89% and >82% for savannah grass and savannah wood and >72% for boreal forest surface, respectively. Previous studies have also found oxygenated species to be a large portion of organic vapor emissions across various biomass fuels (Bruns et al., 2016; Gilman et al., 2015; Koss et al., 2018; Stockwell et al., 2015; Zhu et al., 2021). These OVOCs have important atmospheric implications as their photolysis is an important source of HO_x, which promotes NO-to-NO_2 recycling and thereby drives O_3 production via NO_2 photolysis (Li et al., 2022). OVOCs were also found to be a more important source for BB-derived SOA than heterocyclics, especially at lower (<1 day) aging times (He et al., 2024).

OVOCs were followed by C_xH_y (4-8%) for savannah grass and savannah wood, whereas the C_xH_y fraction was higher for boreal forest surface (14%). ArHCs contributed a smaller fraction (3-5%) for savannah grass and savannah wood but were higher (7%) for boreal forest surface. Previous airborne observation of boreal wildfire plumes reported a hydrocarbon-rich organic vapor composition, with hydrocarbons contributing ~53% of the total measured organic vapors (Hayden et al., 2022). Nitrogen-containing compounds together had ~3-5% contributions to total primary organic vapor emission for savannah fuels and ~7% contribution for boreal forest surface. Phenolic compounds contributed 6-7% to the total primary organic vapor EFs across the fuels. Phenolic compounds are considered as important OH· reactants for the formation of secondary brown carbon formation in BBSOA (Palm et al., 2020). Several dominant compounds were identified based on their contribution to the total EFs across the primary experiments, e.g. furfural ($C_5H_4O_2$; 1.4-12.9%), 4-methoxy-2(5H)-furanone ($C_5H_6O_3$; 0.8-7.1%), acetic acid ($C_2H_4O_2$; 1.8-12.5%), acetic anhydride ($C_4H_6O_3$; 1.5-5.6%), acetone (C_3H_6O; 1.7-5.1%), hydroxy acetone ($C_3H_6O_2$; 1.5-6.1%), $C_2H_6O_3$ (3.7-17.8%). Many of these compounds were also reported in previous BB studies (Bruns et al., 2017; Stockwell et al., 2015; Wang et al., 2025).

3.2 Chemical evolution of organic vapors in the chamber

The evolution of organic vapors classified by functional group classes with eqv. day of aging (standardized to 0.5 eqv. day of aging) for both photochemical and dark aging experiments for savannah grass, savannah wood and boreal forest surface biomass fuel is shown in Figure 2.

At time zero (t=0h), UV lights were turned on for daytime photooxidation with OH· acting as a dominant oxidant, and behavioral changes of each class were observed. In general, OH· reacts with VOCs via three main pathways, including H-atom abstraction, ~~and~~ OH· addition to C=C bonds and OH· addition to aromatic rings, which accelerate the depletion of unsaturated and aromatic classes and drives the formation of more oxygenated products (Ziemann and Atkinson, 2012). During the photochemical aging experiments, the most extensive decay was observed for furanic, phenolic and oxygenated aromatic compounds across the biomass fuels. Furanic compounds especially showed rapid decay immediately after the UV lights were switched on, consistent with fast processing driven by OH· oxidation and potential additional loss via direct photolysis. Furan aldehydes exhibit measurable absorption in the 290-380 nm region (Colmenar et al., 2015).

For savannah grass, furanic compounds showed rapid early loss once UV light was switched on for photochemical aging, and by 0.25 eqv. day of photochemical aging, EFs declined from ~~30.7 to 18.8 g kg^{-1} in Exp. 2 (39% depletion, min) and from~~ 25.7 to 9.6 g kg^{-1} in Exp. 7 (63% depletion, max). Phenolic compounds were depleted more strongly from ~~5.7 to 2.4 g kg^{-1} in Exp. 2 (58% depletion, min) and from~~ 3.4 to 0.8 g kg^{-1} in Exp. 7 (76% depletion, max) during the same early decay (0.25 eqv. day) period. By 0.5 eqv. day of photochemical aging, >75% of furanic and >80% of phenolic compounds were depleted across all the savannah grass experiments (Figure S4), with the greatest overall losses observed in Exp. 7 (Figure 2). Oxygenated aromatics showed similar behavior, declining by ~77-81% by 0.5 eqv. day of photochemical aging with only 0.2 g kg^{-1} remaining by the end of Exp. 7. The large reduction in furanic, phenolic and oxygenated aromatic compounds highlight the highly reactive nature of these species with OH·.

Formatted: Font: 11 pt

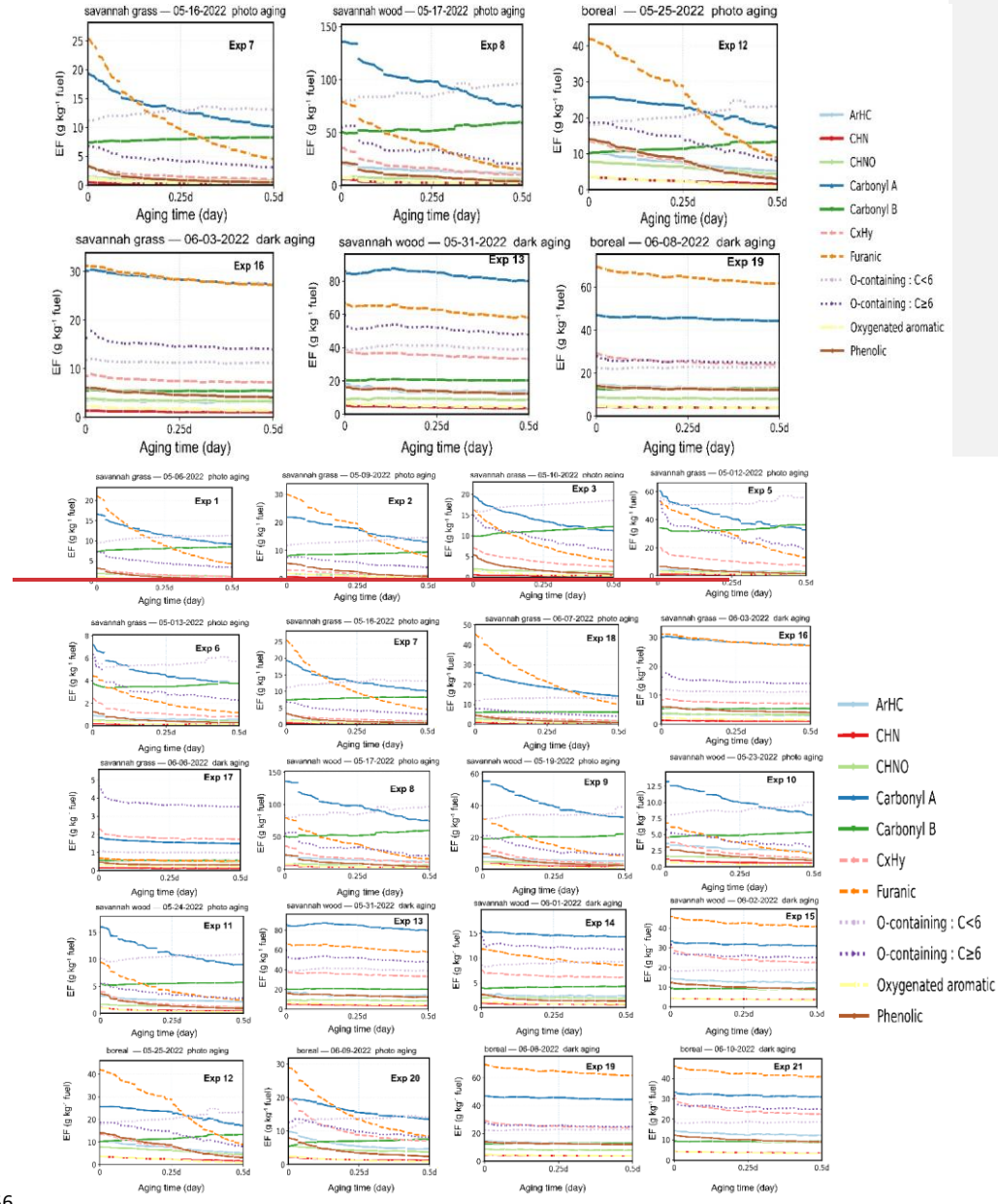
savannah grass — 05-16-2022 photo aging
Exp 7
savannah wood — 05-17-2022 photo aging
Exp 8
boreal — 05-25-2022 photo aging
Exp 12
savannah grass — 06-03-2022 dark aging
Exp 16
savannah wood — 05-31-2022 dark aging
Exp 13
boreal — 06-08-2022 dark aging
Exp 19
EF (g kg⁻¹ fuel)
Aging time (day)
0
0.25d
0.5d
ArHC
CHN
CHNO
Carbonyl A
Carbonyl B
CxHy
Furanic
O-containing : C<6
O-containing : C≥6
Oxygenated aromatic
Phenolic

savannah grass — 05-06-2022 photo aging
Exp 1
savannah grass — 05-09-2022 photo aging
Exp 2
savannah grass — 05-16-2022 photo aging
Exp 3
savannah grass — 05-012-2022 photo aging
Exp 5
savannah grass — 05-013-2022 photo aging
Exp 6
savannah grass — 05-16-2022 photo aging
Exp 7
savannah grass — 06-07-2022 photo aging
Exp 18
savannah grass — 06-03-2022 dark aging
Exp 16
savannah grass — 06-06-2022 dark aging
Exp 17
savannah wood — 05-17-2022 photo aging
Exp 8
savannah wood — 05-19-2022 photo aging
Exp 9
savannah wood — 05-23-2022 photo aging
Exp 10
savannah wood — 05-24-2022 photo aging
Exp 11
savannah wood — 05-31-2022 dark aging
Exp 13
savannah wood — 06-01-2022 dark aging
Exp 14
savannah wood — 06-02-2022 dark aging
Exp 15
boreal — 05-25-2022 photo aging
Exp 12
boreal — 06-09-2022 photo aging
Exp 20
boreal — 06-08-2022 dark aging
Exp 19
boreal — 06-10-2022 dark aging
Exp 21
EF (g kg⁻¹ fuel)
Aging time (day)
0
0.25d
0.5d
ArHC
CHN
CHNO
Carbonyl A
Carbonyl B
CxHy
Furanic
O-containing : C<6
O-containing : C≥6
Oxygenated aromatic
Phenolic

456
457
458

Figure 2. Chemical evolution of organic vapors ~~is~~ categorized by functional groups ~~throughout~~ during aging in the smog chamber. The x~~X~~-axis shows equivalent aging time up to 0.5 eqv. Day, ~~across experiments~~and , y~~Y~~-axis represents emission factors (EFs; g kg^{-1} fuel) ~~in g of emission per kg of biomass fuel burnt~~. One selected photochemical aging experiment and one selected dark aging experiment are shown for each biomass fuel and the remaining experiments are provided in the Figure S4. Aging time t=0 represents when UV light was switched on for photochemical aging experiments or when O_3 was injected for dark-aging experiments.

Formatted: Superscript

Savannah wood experiments also showed ~70-80% depletion for furanic, phenolic and oxygenated aromatic compounds by 0.5 eqv. day of aging across all photochemical aging experiments (Figure S4), with the largest reductions observed in Exp. 8 (Figure 2). For boreal forest surface fuel, only 21% (Exp. 12) ~~and 29% (Exp. 20)~~ of the furanic compounds remained by 0.5 eqv. day of aging. Phenolic compounds and oxygenated aromatics showed comparable depletions with larger reductions (~78%) in Exp. 12. ArHCs including benzene (C_6H_6, *m/z* 79.05), toluene (C_7H_8, *m/z* 93.07), xylenes/ethylbenzene (C_8H_{10}, *m/z* 107.08) declined, with overall reduction of ~33-45% for ArHCs for savannah fuels and >50% for boreal forest surface by 0.5 eqv. day of aging. Aromatic species are susceptible to multiple oxidation pathways and actively drive complex chemical reactions in the atmosphere, strongly governed by OH· reactivity (Ziemann and Atkinson, 2012). C_xH_y compounds also substantially decayed by 65-76% across the biomass fuels. Reductions in the EFs of N-containing compounds were also observed across different experiments. It is important to note that in general, the variability in atmospheric precursor depletion dynamics is highly dependent on differences in oxidant availability, their photochemical reactivity and the chemical composition of the emissions (Georgopoulou et al., 2025; Henze et al., 2008; Liu et al., 2018; Ziemann & Atkinson, 2012).

Subcategories of certain oxygenated classes behaved differently when exposed to photochemical aging. E.g. the EFs of compounds corresponding to the 'carbonyl A' group overall decreased by 40-48% for savannah fuels and 29-33% for boreal forest surface by 0.5 eqv. day with substantial reduction observed for some key carbonyl compounds for e.g. crotonaldehyde (C_4H_5O, *m/z* 70.04), methacrolein or MVK (C_4H_6O, *m/z* 71.04) and acetic anhydride ($C_4H_6O_3$, *m/z* 103.03) decaying by 55-83%, 47-66% and 30-53% across fuels, respectively. In contrast to carbonyl A compounds, photooxidation led to ~3-5 fold higher EFs across fuels for certain acid compounds from 'carbonyl B' for e.g. glycolic acid ($C_2H_4O_3$, *m/z* 77.02) and fumaric acid ($C_4H_4O_4$, *m/z* 117.01), with most of the enhancement observed already by 0.25 eqv. day of aging. These C_2-C_4 aliphatic oxygenates were also observed in the day-time aged plume at an urban site several hours downwind of the wildfires in a previous study ~~by~~ (Liang et al, 2022b). Toxicological evidence has identified gaseous carbonyl compounds as critical contributors to the adverse biological effects of wood combustion emissions (Dilger et al., 2023) , and short-lived unsaturated carbonyls have been shown to drive cellular responses as toxic constituents (Han et al., 2020). Carbonyl A contains unsaturated carbonyls being strong electrophiles, such as acrolein and redox-active quinones potentially inducing oxidative stress, such as benzoquinone, whereas carbonyl B is more dominated by small acids. Given the steady increase of carbonyl B and decrease of carbonyl A, both the inhalation hazard and risk concerning the compound class of volatile carbonyls is reduced by atmospheric aging.

The enhancement of the oxygenated compounds, particularly organic acids~~s~~e and other secondary oxidation products ~~secondary organic vapors~~ belonging to the carbonyl B class, e.g. acetic acid ($C_2H_4O_2$, *m/z* 61.02), succinic

anhydride ($C_4H_4O_3$, *m/z* 101.02), pyruvic acid ($C_3H_4O_3$, *m/z* 89.02) and acetone (C_3H_6O, *m/z* 59.04), was concurrent with the decline in several reactive primary organic vapor classes, suggesting their potential to act as precursors for secondary carbonyl production. Succinic anhydride ($C_4H_4O_3$), a compound with structural similarity with maleic anhydride, is identified as an important secondary organic vapor formed from multigenerational chemistry (Coggon et al., 2019). Previous studies have shown that secondary OVOCs were generated as oxidation products of ArHCs, phenol and furans during aging experiments (Coggon et al., 2019; Liu et al., 2019).

Photooxidation of toluene generates oligomeric oxygenated organic products and small dicarboxylic acids (Sato et al., 2007; Zhang et al., 2024) and has been reported as a potential source of SOA in urban air (Sato et al., 2007). Furans have further been identified as highly OH·-reactive BB organic vapors whose oxidation contributes to the formation of secondary OVOCs, including anhydrides and small acids (Coggon et al., 2019). To understand the role of such key precursors in secondary OVOCs formation, we performed the correlations analysis between toluene or furan, and formic acid ($C_1H_2O_2$), glycolic acid ($C_2H_4O_3$), fumaric acid ($C_4H_4O_4$) and succinic anhydride ($C_4H_4O_3$) mixing ratios for photochemical aging experiments (Figure S7~~3~~).

Across all fuels, those OVOCs exhibited strong negative correlations with toluene and furan. Excluding an anomalous boreal forest surface case on 2022-05-25 for succinic anhydride ($C_4H_5O_3$), R ranges for formic acid were −0.96 to −0.48 /−0.96 to −0.48, glycolic acid were−0.99 to −0.87/−1.00 to −0.95, fumaric acid were −0.98 to −0.75/−0.99 to −0.75, and succinic anhydride were −0.93 to −0.59 / −0.95 to −0.68 for toluene and furan, respectively. Additionally, degradation of formed SOA can also act as a source for these and other volatile organic acids (Malecha and Nizkorodov, 2016). O-containing compounds also showed distinct behavior based on the number of carbon present, and compounds containing C≥6 showed a net decrease of 47-66% for savannah fuels and 35-57% for boreal forest surface by 0.5 eqv. day of photochemical aging. On the other hand, O-containing compounds containing C<6 showed overall enhancement of 11-32% across photochemical aging experiments for savannah fuels, except ~~experiment 6~~Exp. 6 (no net change), and relatively higher 32-37% overall enhancement across photochemical aging experiments for the boreal forest surface fuel. We compared the average total organic vapor EFs for the fresh and aged emissions across different experiments. Although an increase in the average total organic vapor EFs would be expected after photochemical aging due to the formation of certain oxygenated subclasses (carbonyl B, O-containing compounds C<6) from reactive primary organic vapors discussed above, the average total organic vapor EFs after aging were reduced by 5-20% for savannah wood, and 22-32% for boreal forest surface, while for savannah grass, it showed mixed trends with reduction of 27-34% in Exp. 1,2,7 and 18, while a relative increase of ~25% in Exp.~~exp~~ 3,5 and 6 with respect to their average total primary EFs. It is important to consider that the wall losses of organic vapors to chamber walls can lead to a reduction in total organic vapor concentration. Hartikainen et al. (2018) estimated that, owing to the considerably larger size and low surface-to-volume ratio (29 m3) of ILMARI chamber, losses of organic vapor to the chamber walls are expected to be relatively small compared with condensation onto particles. ~~,~~ Conversely, ~~while in parallel~~ oxidation can transform compounds that were initially undetected by PTR-MS (e.g. alkanes) into more oxygenated products that fall within the PTR-MS detection range, as opposite effect. Additionally, particle-phase processes, such as condensation/evaporation and reactive uptake of gases can also influence the gas-phase behaviour. A detailed analysis of SOA formation and multiphase processes will be addressed in a separate study.

In contrast to the prominent effect of photochemical aging, with rapid changes in the composition of organic vapors in the chamber across all the photochemical aging experiments, the dark aging experiments of BB did not show

substantial changes. Phenolic compounds, which react rapidly with $NO_3\cdot$, showed negligible or only minor reductions in EFs during dark aging experiments, similar to other organic vapor classes. This suggests that $NO_3\cdot$ formation was limited under our experimental conditions, and the observed evolution of organic vapors is dominated by weak O_3 oxidation for dark aging experiments. This is in contrast with previous dark aging studies of residential BB emissions where NO_3-driven oxidation resulted in substantial SOA production (Kodros et al., 2022).

The difference in the behavior of organic vapors in different oxidation regimes is related to variability in precursors' reactivity with the oxidants and their effective loss rates, which are governed by the corresponding pseudo-first-order rate constants. Since most VOCs have higher reaction rates with OH· than with O_3, it is expected that the oxidation process in the chamber is mainly driven by OH· (Li et al., 2023). O_3 exhibits negligible reactivity (Ziemann and Atkinson, 2012) with alkanes, other saturated VOCs and simple aromatics such as benzene and alkylated benzene ($k \lesssim 10^{-23}$–10^{-20} cm^3 $molecule^{-1}$ s^{-1} at 298 K). Therefore, reactions with these compounds are slow, and their lifetimes with respect to O_3 are orders of magnitude longer than their lifetime with respect to other oxidants (Atkinson, 2000).

However, for BB-related ArHC such as styrene and unsaturated HCs, especially for many terpenes, O_3 can be an important oxidant. A recent chamber study on BB emissions similarly showed that the reactions with OH· are the dominant daytime oxidation pathway for most VOCs, while O_3-induced oxidation was a minor consumption mechanism for most species (k_{O3}= 10^{-17}–10^{-22} cm^3 $molecule^{-1}$ s^{-1}), with the main exception of monoterpenes and their fragments, for which O_3 was important (Georgopoulou et al., 2025).

The relative share of each class (Figure S5) shows a compositional shift similar to that observed in the EF_S trends discussed above. The relative share of classes in fresh emissions was compared to their relative share in different aging emissions. For experiments later subjected to photochemical aging, the primary emissions were associated with high emissions of carbonyl A, with a range of 20-28% relative share for savannah grass, 27-30% for savannah wood and 15% for boreal forest surface. This was followed by furanic compounds with 25-44% relative share for savannah grass, 16-21% for savannah wood and 25-27% for boreal forest surface. On exposure to photochemical aging over 0.5 eqv. day, their relative share reduced to 10-30% for savannah grass, 9-11% for savannah wood and 17-18% for boreal forest surface while the relative share of carbonyl B increased from 6-7% to 12-15% for savannah wood, from 4-7% to 8-17% for savannah grass and from 3-5% to 7-11% for boreal forest surface after photooxidation. The relative share of O-containing compounds with C<6 nearly doubled across biomass fuels. For dark aging experiments, the shifts for most compound classes were subtle, but the O-containing compounds with C≥ 6 were found to be increasing on a relative scale from 7-13% to 13-34% for savannah grass, from 7-8% to 14-19% for savannah wood, and from 7-8% to 11-14% for boreal forest surface.

3.3 Cluster analysis of organic vapor composition

We performed a cluster analysis to examine whether the broad organic vapor composition co-varies with experimental factors (fuel, oxidation regime, MCE). A cluster map was constructed as shown in Figure 3 to visualize samples and groups that share similar composition patterns. The cluster map comprises a central heatmap accompanied by row and column dendrograms, which summarize similarities among variables (compound groups) and observations (samples; date x fuel x oxidation regime), respectively.

Formatted: Font: 11 pt

577 The group-level mixing ratios were auto scaled by sample (column), thus, the heatmap colors indicated, within
578 each sample, relative enrichment/depletion of each compound group compared to that sample's mean. For both
579 row and column dendrogram in the cluster map, the cophenetic coefficients (r) were 0.88 (row) and 0.92 (column),
580 indicating good representation of the pairwise distances within variables and within observations and supporting
581 interpretation of the branch structure. On this relative composition scale, samples separated primarily by oxidation
582 regime, with UV+O_3 forming a distinct cluster in the dendrogram corresponding to a unique compositional regime,
583 while fresh and O_3 remained comparatively close. Regime centroids in the composition space supported this
584 interpretation (Fresh-O_3= 0.67, Fresh-UV+O_3=3.10, and O_3-UV+O_3=2.64).
585

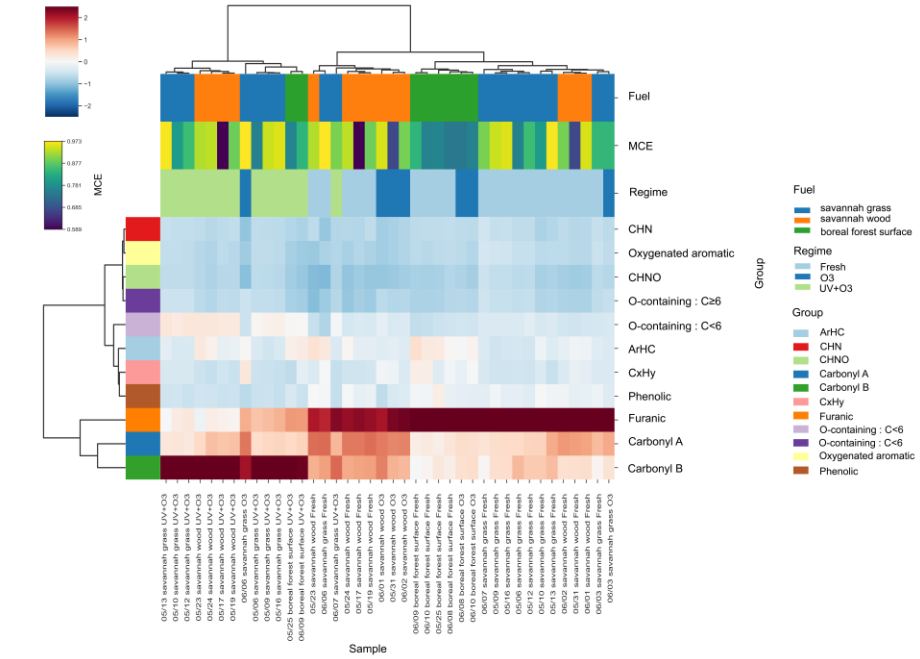
MCE
Fuel
MCE
Regime
CHN
Oxygenated aromatic
CHNO
O-containing : C≥6
O-containing : C<6
ArHC
CxHy
Phenolic
Furanic
Carbonyl A
Carbonyl B
Group
Fuel
savannah grass
savannah wood
boreal forest surface
Regime
Fresh
O3
UV+O3
Group
ArHC
CHN
CHNO
Carbonyl A
Carbonyl B
CxHy
Furanic
O-containing : C<6
O-containing : C<6
Oxygenated aromatic
Phenolic
Sample

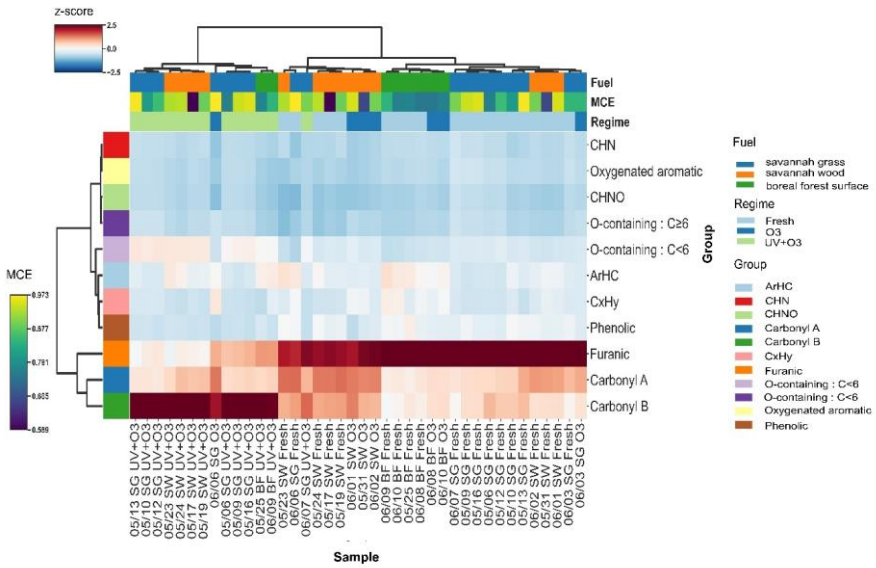
z-score
MCE
Fuel
MCE
Regime
CHN
Oxygenated aromatic
CHNO
O-containing : C≥6
O-containing : C<6
ArHC
CxHy
Phenolic
Furanic
Carbonyl A
Carbonyl B
Group
Fuel
savannah grass
savannah wood
boreal forest surface
Regime
Fresh
O3
UV+O3
Group
ArHC
CHN
CHNO
Carbonyl A
Carbonyl B
CxHy
Furanic
O-containing : C<6
O-containing : C<6
Oxygenated aromatic
Phenolic
Sample

586

Figure 3. Hierarchically clustered heatmap of standardized mean mixing ratios grouped by compound groups (rows) and regime-resolved samples (columns; date x fuel x regime), with row and column dendrograms summarizing similarities among compound groups and regime-resolved samples, respectively. Columns represent individual samples across fresh, dark aging (O_3) and photochemical aging ($UV+O_3$) regimes for savannah grass (SG), savannah wood (SW) and boreal forest ~~surface~~(BF) surface. Values are sample-standardized z-scores (each column z-scored to mean =0, SD=1), so heatmap colors indicate relative enrichment (red) or depletion (blue) of a compound group within that sample. Column color tracks denote fuel (biomass type), MCE (modified combustion efficiency, continuous gradient), and regime, while row colors indicate compound groups. Strongest effect in clustering of standardized compositions were observed for the factor Aging Regime, particularly between "$UV+O_3$" and "Fresh" / "O_3", followed by Fuel but no apparent effect by MCE.

The influence of fuel was less evident than photochemical aging, nevertheless clear compositional fingerprints across regimes. Savannah wood and savannah grass clustered more closely together, while boreal forest surface fuel generally separated, indicating compositionally distinct behavior. The heatmap revealed fuel-specific fingerprints that persisted across regimes. In the sample-standardized (column-z-scored) composition space, boreal forest surface exhibited a furanic/aromatic-leaning profile with carbonyl depletion. Across regime averages, furanic (+0.44z), ArHC (+0.25z) were elevated, while carbonyl A (-0.33z) and B (-0.41z) were suppressed. Savannah grass exhibited more oxygenated profile with elevated CHNO (+0.09z) and O-containing classes (+0.08-0.10z), with carbonyl B (+0.24z) becoming prominent upon aging. Savannah wood was carbonyl rich and furanic-poor, where carbonyl A (+0.38z) and B (+0.18z) were elevated while furanic compounds were reduced (-0.30z). Thus, fuel sets the baseline composition while regime modulates it, notably $UV+O_3$ pushes the mixture towards oxygenated functionality to a greater extent than O_3 alone, which is in line with the previous section. PERMANOVA confirmed that oxidation regime explained most of the variance, whereas fuel played a smaller role (Table S~~8~~5). Across all samples, regime accounted for 73% of the variance in group-level composition (R^2 = 0.73, F =50.3, p = 0.001), while fuel explained only 10% (R^2= 0.10, F=2.08, p= 0.114). Within each fuel, regime remained highly significant and explained 73-96% of the variance (R^2= 0.73-0.96, all p= 0.001 for savannah grass and savannah wood, p= 0.01 for boreal forest surface), confirming that photochemical aging drives a coherent compositional shift superimposed on fuel-specific baselines. Although there was a strong negative correlation between MCE and absolute ΣEF_{VOC} (Vakkari et al., 202~~6~~5), it did not structure the relative composition space used for clustering based on the normalized compositional data. A Mantel test showed no association between composition distance and $|\Delta MCE|$ ($\rho = -0.003$, p = 0.531).

3.4 Molecular-level characteristics

Formatted: Font: 11 pt

In Figure 4a, emitted compounds are separated according to their carbon number along the x-axis. The dominant signals in organic vapors for savannah wood, savannah grass and boreal forest surface biomass fuels were attributed to C_2-C_6 compounds, with dominant signals of C_5 compounds in fresh emissions. Compared to savannah fuels, boreal forest surface showed more species with higher carbon numbers ($C \geq 9$). Under dark aging experiments, the dominant signals were still concentrated within C_2-C_6 compounds across the biomass fuels. For photochemical aging, the dominant signal of C_2 alone accounted for 28% of the total organic-vapor signal for savannah grass, 31% in savannah wood and nearly 20% in boreal forest surface. The lower carbon number shift after photochemical aging indicates the rapid oxidation of condensable gases prior to those gases having time to condense on particles,

leading to fragmentation. However, other processes such as photolysis and heterogenous photooxidation of pre-existing particle mass, leading to fragmentation and evaporation (Palm et al., 2016), may also result in the production of small gas-phase molecules. The bin containing hydrogen-to-carbon ratios (H/C) >1.7 had the highest contribution across biomass fuels, with the highest contribution in savannah wood ranging from 33% in primary emission to 40% under dark aging and relatively higher, i.e. 59%, under photochemical aging. The addition of OH· to aromatic rings and subsequent ring opening can increase H/C relative to primary emissions during gas-phase oxidation (Liang et al., 2024). Oxygen-to-carbon ratios (O/C) presented in Figure 4b showed moderately oxidized vapors (O/C= 0.5-0.7) contributed significantly to savannah fuels in both primary and dark aging experiments. In contrast, boreal forest surface emissions showed a more substantial low-oxygen fraction (O/C <0.15) in primary (28%) and dark aging (24%), consistent with a high proportion of C_xH_y compounds. Photochemical aging led to the formation of more oxygenated organic vapors with a high contribution of species with O/C >0.7, reflecting enhanced oxidative functionalization in savannah fuels (38%) and boreal forest surface biomass fuel (26%). Under dark aging, however, a substantial low-oxygen fraction (O/C < 0.15) was retained. This contrast between photochemical and dark aging is consistent with a chamber study by Cheung et al., 2025which showed OH-driven photooxidation produced much more oxidized aerosol than dark aging experiments.

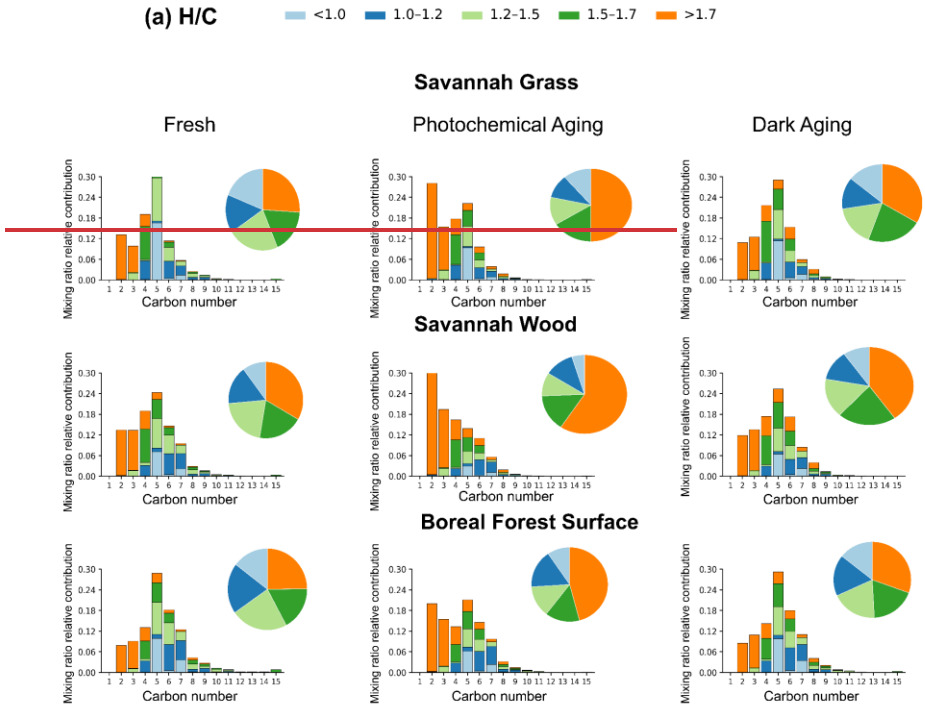
(a) H/C
<1.0
1.0–1.2
1.2–1.5
1.5–1.7
>1.7
Savannah Grass
Fresh
Photochemical Aging
Dark Aging
Savannah Wood
Boreal Forest Surface
Mixing ratio relative contribution
Carbon number

641

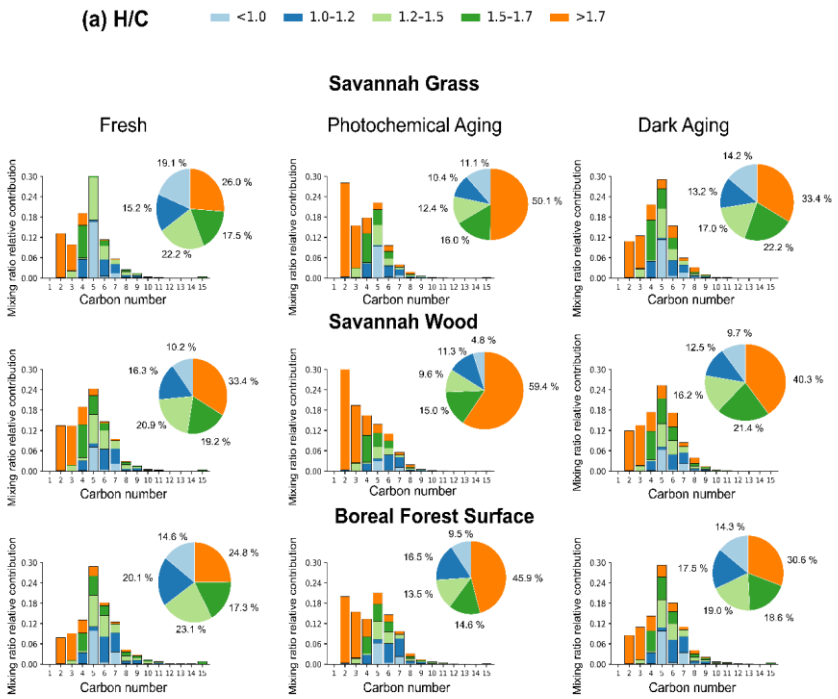
(a) H/C
<1.0
1.0-1.2
1.2-1.5
1.5-1.7
>1.7
Savannah Grass
Fresh
Photochemical Aging
Dark Aging
Savannah Wood
Boreal Forest Surface
Mixing ratio relative contribution
Carbon number
19.1 %
26.0 %
15.2 %
17.5 %
22.2 %
11.1 %
10.4 %
50.1 %
12.4 %
16.0 %
14.2 %
13.2 %
33.4 %
17.0 %
22.2 %
10.2 %
16.3 %
33.4 %
20.9 %
19.2 %
4.8 %
11.3 %
9.6 %
59.4 %
15.0 %
9.7 %
12.5 %
40.3 %
16.2 %
21.4 %
14.6 %
24.8 %
20.1 %
17.3 %
23.1 %
9.5 %
16.5 %
45.9 %
13.5 %
14.6 %
14.3 %
30.6 %
17.5 %
19.0 %
18.6 %

642

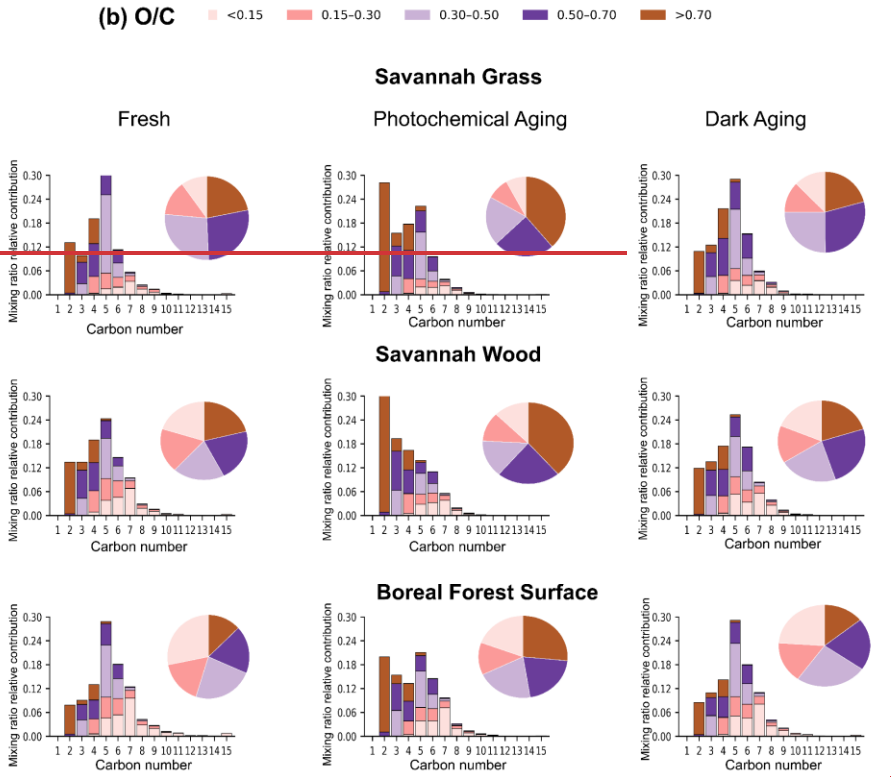
(b) O/C
<0.15
0.15–0.30
0.30–0.50
0.50–0.70
>0.70
Savannah Grass
Fresh
Photochemical Aging
Dark Aging
Savannah Wood
Boreal Forest Surface
Mixing ratio relative contribution
Carbon number

643

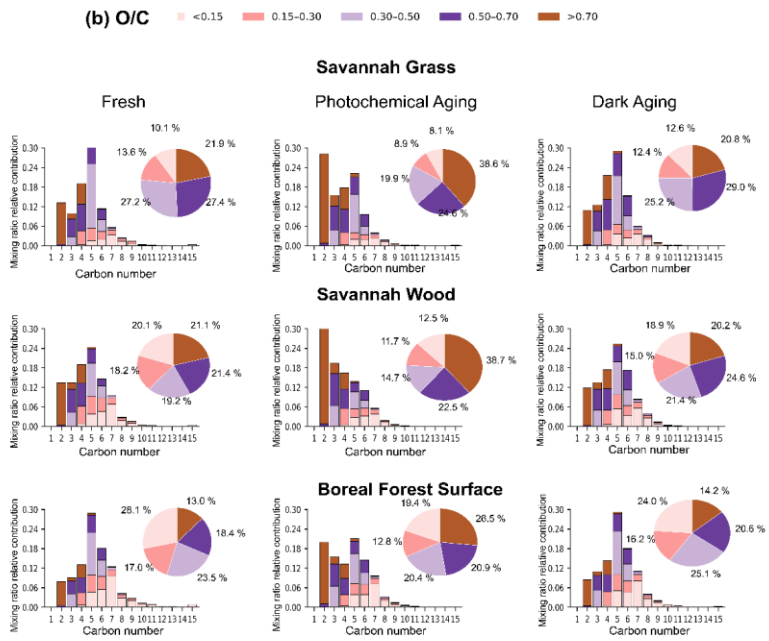

Figure 4. The average carbon distribution for savannah grass, savannah wood and boreal forest surface across fresh, photochemical aging and dark aging colored by (a) H/C and (b) O/C. The pie charts are the corresponding contributions by H/C and O/C ratios for each regime.

Based upon the elemental composition, molecular formulas were assigned to C_xH_y, $C_xH_yO_z$ ($z<3$ and $z\geq3$), $C_xH_yN_i$ and $C_xH_yO_zN_i$ categories for their bulk-level characterization (Figure 5). In fresh emissions, $C_xH_yO_z$ ($z<3$) was the dominant class, contributing approximately 52-59% of the total relative contribution, followed by $C_xH_yO_z$ ($z\geq3$) (20-28%) across biomass fuels. Photochemical aging increased the mean relative contribution of $C_xH_yO_z$ ($z\geq3$) from 22.7 ± 1.8% to 34.6 ± 1.2% in savannah wood, from 27.7 ± 3.6% to 37.3 ± 1.2% in savannah grass, and from 19.9 ± 1.0% to 29.9 ± 1.8% in boreal forest surface. ~~In primary emissions, $C_xH_yO_z$ ($z<3$) comprised of 53-61% of total mean mixing ratio (ppbv), followed by $C_xH_yO_z$ ≥3 (20-29%), C_xH_y (7-21%), and $C_xH_yN_i$ (1-3%) and $C_xH_yO_zN_i$ (2-4%). Photooxidation led to an increase in $C_xH_yO_z$ ($z\geq3$) fraction from 23% in primary emission to 31% after photooxidation in savannah wood, 29-35% in savannah grass and 20 to 27% in boreal forest surface.~~ High oxygen numbers in larger compounds relate to low volatilities that promote condensation on pre-existing surfaces, favor new particle formation and contribute to subsequent growth of newly formed particles, hence enhancing SOA formation (Ahern et al., 2019; Akherati et al., 2020; He et al., 2024). The mean mixing ratio distributions under fresh, photochemically aged and dark-aged conditions were largely centered at DBE values between 0 and 4. Photochemical aging shifted the distribution towards the lower DBE (particularly DBE =0-1) as presented in

Figure S62. Organic vapors with a relatively low DBE are known to originate from oxidation of aliphatic precursors (An et al., 2024). High C_xH_y in boreal forest surface is consistent with findings discussed in previous section.

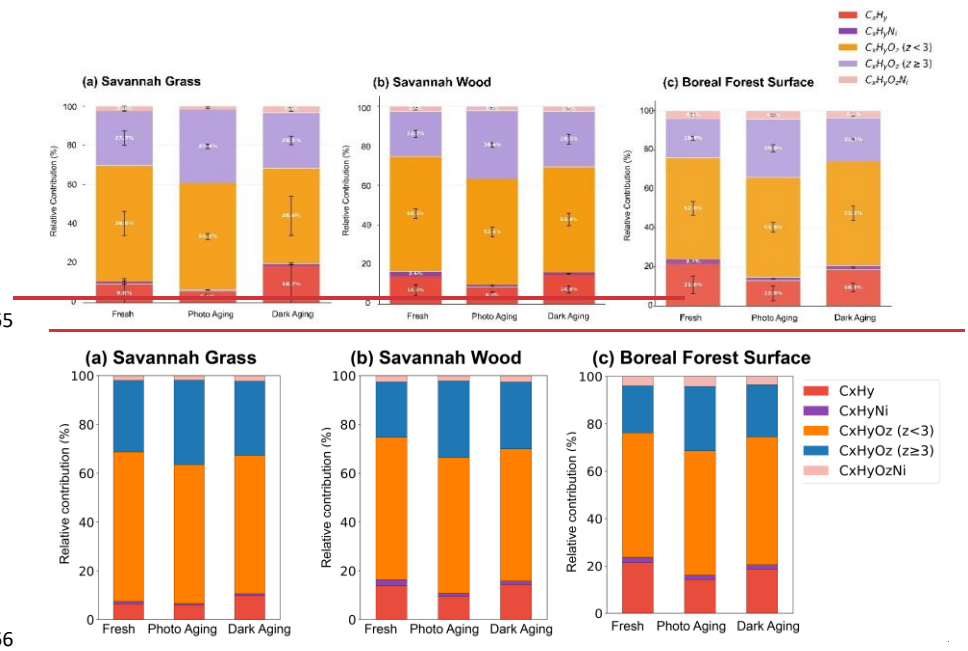

Figure 5. Stacked bar plots showing the mean relative contribution (%) of compound classes (C_xH_y, $C_xH_yO_z$ (z<3), $C_xH_yO_z$ (z≥3), $C_xH_yN_i$ and $C_xH_yO_zN_i$) to the total mean mixing ratio (ppbv) for (a) savannah grass, (b) savannah wood and (c) boreal forest surface ~~across~~ under fresh, photochemical aging and dark aging ~~regimes~~conditions. Error bars indicate the standard deviation; n = 9, 7 and 2 (savannah grass); n= 7,4 and 3 (savannah wood) and n= 4, 2 and 2 (boreal forest surface) for fresh, photo aging and dark aging conditions.

Kendrick mass defect (KMD) plots (CH_2 base) for individual molecular formulas detected in fresh and aged emission for savannah grass, savannah wood and boreal forest surface show fresh emissions clustering at low-mid *m/z* with KMD ≈ 0.02–0.10, indicating dominance of lightly oxygenated CHO series immediately after emission (Figure 6). The most intense fresh formulas were $C_5H_4O_2$ (furfural; *m/z* 97.02), $C_2H_4O_2$ (acetic acid; *m/z* 61.02), $C_5H_6O_3$ (4-methoxy-2(5H)-furanone; *m/z* 115.040), $C_3H_6O_2$ (hydroxy acetone; *m/z* 75.045), and $C_2H_6O_3$ (*m/z* 79.04). Horizontal alignment along the KMD band indicates a homologous series with shared backbones differing by CH_2 and was consistent across fuels. Dark aging produced modest increases for O-containing compounds with C≥6, i.e. $C_6H_{12}O_3$ (*m/z* 133.08) across the biomass fuels, $C_6H_{10}O_2$ (*m/z* 115.076), and C_5H_8 hydrocarbon (e.g. isoprene or cyclopentene; *m/z* 69.07) for savannah fuels, alongside depletions of fresh dominant formulas such as $C_5H_4O_2$, $C_5H_6O_3$ and $C_2H_4O_2$. In boreal forest surface emission, C_3H_6O (acetone; 59.05) and $C_2H_6O_3$ (*m/z* 79.04) were enhanced. This pattern is consistent with selective ozonolysis of unsaturated olefinic and furanic precursors,

where compounds containing C=C bonds are rapidly oxidized to a limited set of oxygenated products while others are consumed. O_3 preferentially reacts with C_6–C_7 olefinic hydrocarbons (e.g., C_6H_8, C_7H_{10}) and terpenoid fragments resulting in their depletion across fuels. Similarly, furanic compounds such as $C_5H_4O_2$ (furfural) and $C_5H_6O_3$ (furanone) also decreased through O_3 attack on the unsaturated furan ring.

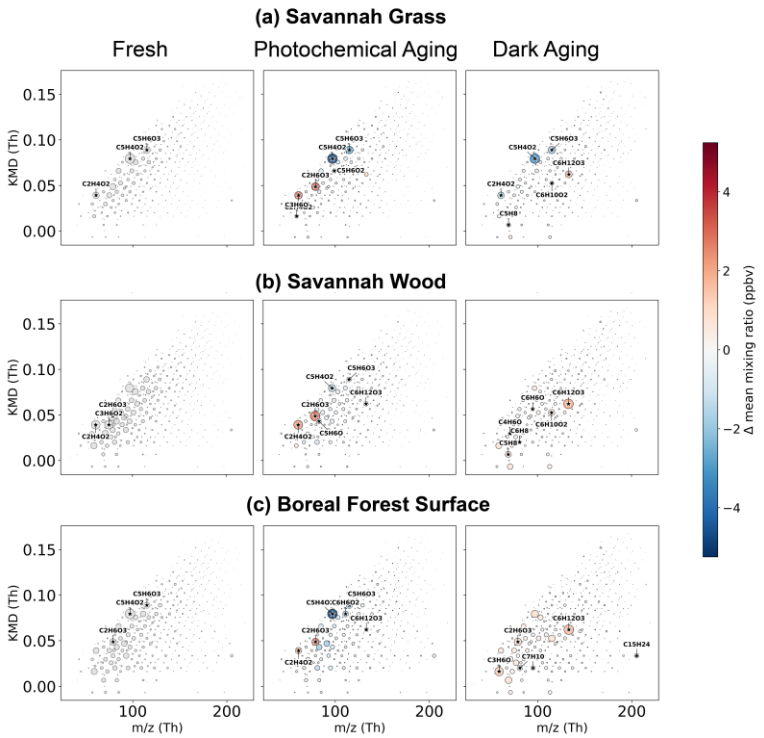

Figure 6. Kendrick mass-defect (KMD) plots for savannah grass, savannah wood and boreal forest surface across fresh, dark aging (Δ O_3) and photochemical aging (UV+Δ O_3). In fresh panel, marker size ∝ to mean mixing ratio (ppbv), normalized within each biomass. In aging panels, marker size ∝ |Δ|= $ppbv_{aged}$–$ppbv_{fresh}$. Colors in aged panels encode the signed change on a global, symmetric scale: red = increase, blue = decrease (color intensity scales with |Δ|). Top-changing species are indicated by black star markers and bold labels with a white outline.

Photooxidation (UV+O_3) drives larger, more coherent increases in mean mixing ratios centered at *m/z* ~60–150 and KMD ≈ 0.04–0.10, producing smaller, more oxygenated products across all fuels via a combination of fragmentation and functionalization reactions. Consistently, $C_2H_6O_3$ (*m/z* 79.040) and $C_2H_4O_2$ (acetic acid; *m/z* 61.029) increased substantially. Enhancement for C_3H_6O (acetone; *m/z* 59.05) for savannah grass was also observed. The largest reduction occurred for $C_5H_4O_2$ (furfural; *m/z* 97.029) across the biomass fuels followed by $C_5H_6O_3$ (4-methoxy-2(5H)-furanone; *m/z* 115.040), indicating rapid conversion of primary C_5-furanics compounds into smaller oxygenates. Prior smog chamber studies have examined oxidation of furan and methyl-substituted furans, and their

Formatted: Justified, Line spacing: 1.5 lines

reaction intermediates have been examined for SOA yields (Ali et al., 2024; Strollo & Ziemann, 2013; Tajuelo et al., 2021; Yuan et al., 2017b). However, furanic compounds with additional oxygen-containing substituents have been examined far less, and in our study, they were rapidly transformed during photooxidation. The modest increase in some higher-mass oxygenates is consistent with limited functionalization, whereas the strong, coherent rise in mean mixing ratios of C_2-C_3 oxygenates, alongside depletion of C_5-furanic compounds, suggests fragmentation-dominated chemistry. –This fragmentation-dominated aging modulates radical (HO_x) and O_3 chemistry while generating oxygenated products that can undergo further oxidation and may contribute to SOA formation.

~~and contributes to seed later SOA.~~

4 Conclusions

This work provides a detailed chemical characterization of BB organic vapors from a series of controlled laboratory burns. We characterized organic vapor EFs from globally relevant savannah and European boreal forest surface biomass fuels, using a high-resolution PTR-MS and investigated their transformation under photochemical and dark aging experiments in a smog chamber. Primary emissions varied considerably between the biomass fuels, with the highest average total organic vapor EF (160.8 g kg^{-1}) observed for European boreal forest surface biomass and the lowest (69.1 g kg^{-1}) from savannah grass. These differences largely reflected variations in MCE together with glowing combustion cases for savannah grass contributing to its lower overall EFs. In general, lower MCE values resulted in higher emissions of organic vapors, consistent with previous BB studies. The total organic vapor EFs reported here are generally higher than the values reported in previous studies (Gkatzelis et al., 2024; Koss et al., 2018; Permar et al., 2021; Travis et al., 2023). This difference reflects the broader molecular coverage achieved in the present study, where approximately 3–4 times more ions were considered.

Previous studies have emphasized the importance of VOCs emitted from BB in driving atmospheric oxidation chemistry and secondary pollutant formation (Jin et al., 2026; Zhu et al., 2021). However, molecular-level characterization of gas-phase organic compounds from savannah wildfires remains limited, and studies of boreal BB have largely focused on North American ecosystems, with rare investigations on European boreal forest.

In the present study, primary emissions were dominated by small OVOCs such as furanic, carbonyl A and O-containing compounds with C<6 across the biomass fuels, with boreal forest surface exhibiting higher hydrocarbon (C_xH_y) fractions and relatively more high-carbon species (C≥9). Across biomass fuels and regimes, $C_xH_yO_z$ (z<3) accounted for ~53–61% of the total organic vapor composition. Elemental and molecular composition analysis revealed that fresh vapors were moderately oxidized, and under photooxidation of 0.5 eqv. day, the vapors shifted towards higher O/C (>0.70) with an increased fraction of $C_xH_yO_z$ ($z \geq 3$), alongside the formation of lower-carbon products, indicating concurrent functionalization and fragmentation processes.

Photochemical aging produced pronounced compositional changes in organic vapors, whereas dark aging under low-NO_x conditions resulted in minimal changes. This indicates that under our experimental conditions, OH·-driven photochemical oxidation exerted a more substantial influence on gas-phase organic composition than O_3-driven dark oxidation. Hierarchical clustering of relative composition reflected this regime-dependence, with photochemical aging (UV+O_3) forming a distinct cluster, while fresh and dark aging (O_3) conditions were relatively similar. PERMANOVA showed a clear hierarchy of control on group-level organic vapor composition, with oxidation regime being the dominant driver and accounting for 73% of the variance, whereas fuel played a secondary role, and MCE exerted the weakest influence on the relative compositional structure. Under

Formatted: Font: 12 pt

Formatted: Normal, Right: 0.16 cm, No bullets or numbering

photooxidation, major BB SOA precursors were substantially depleted. This included substantial loss of furanic, phenolic and oxygenated aromatic compounds by 0.5 eqv. day of aging, with declines of ~70-82%, ~68-86% and ~67-81% across the experiments, respectively. Previous BB laboratory studies show that phenolic compounds have SOA yield of 24-44% (Yee et al., 2013), while furanic compounds have been reported to produce SOA yields of up to 16% (Romanias et al., 2024)Together with the substantial depletion observed during photooxidation in our study, these findings support the need to account for non-traditional precursors, particularly furanic and phenolic compounds, in SOA models to more accurately represent SOA formation from BB emissions. ~~These losses underscore the need to account for non-traditional precursors, particularly furanic and phenolic compounds in SOA models to more accurately represent SOA formation from BB emissions.~~ Subcategories of oxygenated compounds exhibited distinct evolutions in the chamber, with pronounced increases observed for carbonyl B compounds such as glycolic acid ($C_2H_4O_3$, *m/z* 77.02), fumaric acid ($C_4H_4O_4$, *m/z* 117.01), acetic acid ($C_2H_4O_2$, *m/z* 61.02), succinic anhydride ($C_4H_4O_3$, *m/z* 101.02), and acetone (C_3H_6O, *m/z* 59.04), alongside increases in O- containing compounds with C<6. This coincided with a decline in primary reactive organic vapors, suggesting that they are likely precursors to secondary oxygenate formation. Specifically, furan and toluene showed a strong negative correlation with carboxylic acids and succinic anhydride, implying their role in the formation of secondary OVOCs.

Certain limitations should be considered when interpreting the results of these chamber experiments in context to real atmospheric BB plumes. Chamber studies allow controlled investigation of aging processes but may not fully capture the complexity of real atmospheric conditions. Variability in fuel composition and moisture content, plume dilution rates, temperature, background aerosol concentrations, and potential chamber wall losses may affect the emission chemistry. In addition, although representative biomass fuels were collected from the field, combustion was performed under controlled laboratory conditions. Consequently, the experiments cannot fully reproduce the complexity of natural wildfires, including fire spread, plume dynamics, interactions between the fire and the surrounding vegetation and soil, and variability in dilution rates, all of which may influence BB emissions under ambient conditions (Akagi et al., 2011; Hodshire et al., 2019). Therefore, the findings should be interpreted as mechanistic insights obtained under controlled laboratory conditions, and caution should be exercised when comparing them with natural wildfire plumes.

~~A~~In ~~a~~additionally, while PTR-MS provides high-sensitivity, real-time measurements of organic vapors, it cannot reliably distinguish between structural isomers, which may introduce some uncertainties in compound identification without complementary separation techniques. Furthermore, the compositional analysis and discussion presented in this study are based on the assigned molecular formulas. Therefore, the results should be interpreted within the context of these limitations. Another important aspect to consider is that BB plumes in atmosphere undergo repeated cycles of daytime and nighttime oxidation during transport and plumes may experience multi-day aging that can alter their chemical composition. Future studies should therefore investigate longer-aging timescales and successive oxidation regimes, integrating field observations with complementary analytical techniques to better capture the atmospheric evolution of BB plumes and improve their representation in air quality and climate models.

Overall, the collective evidence from elemental ratios, carbon-number distributions, Kendrick mass-defect analysis, and compositional clustering in this study converges on a coherent mechanistic picture that photooxidation drives fragmentation-dominated chemistry (with some functionalization), transforming furanic and aromatic precursors into smaller, more oxygenated, and potentially condensable products of decreased vapor pressure. These results highlight the integral role of OH·-driven photooxidation overcoming differences in BB

emission composition caused by fuel type and combustion conditions and provide critical insight into their atmospheric evolution and molecular characteristics.

Acknowledgements

This project was supported by the Research Council of Finland (grant no 337550, 343359, 341597, 346371, 364229) and by the European Commission under the Horizon 2020 – Research and Innovation Framework Programme, H2020-INFRAIA-2020-1, Grant Agreement No.: 101008004.

Data availability

The data is available from the data repository of the Finnish Meteorological Institute (FMI) at https://doi.org/10.57707/fmi-b2share.hvdp0-qtj25.

Competing interests

The authors also have no competing interests to declare.

Author contributions

DS: data curation, formal analysis, investigation, visualization, writing – original draft preparation; LV: data curation, formal analysis, investigation, writing – review and editing; MI: investigation, methodology; MS: investigation, writing – review and editing; HC: supervision, writing – review and editing; SiSc: funding acquisition, investigation, supervision, writing – review and editing; AB: investigation; IP: investigation, writing – review and editing; KJ: investigation; KK: investigation, writing – review and editing; VL: investigation; PYP: investigation; SJS: investigation, writing – review and editing; PGVZ: funding acquisition; AV: funding acquisition, writing – review and editing; VV: conceptualization, data curation, funding acquisition, investigation, project administration, supervision, writing – review and editing; OS: conceptualization, funding acquisition, resources, supervision, writing – review and editing; RZ: funding acquisition, supervision, writing – review and editing.

References

Ahern, A. T., Robinson, E. S., Tkacik, D. S., Saleh, R., Hatch, L. E., Barsanti, K. C., Stockwell, C. E., Yokelson, R. J., Presto, A. A., Robinson, A. L., Sullivan, R. C., and Donahue, N. M.: Production of Secondary Organic Aerosol During Aging of Biomass Burning Smoke From Fresh Fuels and Its Relationship to VOC Precursors, Journal of Geophysical Research: Atmospheres, 124, 3583–3606, https://doi.org/10.1029/2018JD029068, 2019.

Akagi, S. K., Yokelson, R. J., Wiedinmyer, C., Alvarado, M. J., Reid, J. S., Karl, T., Crounse, J. D., and Wennberg, P. O.: Emission factors for open and domestic biomass burning for use in atmospheric models, Atmos. Chem. Phys., 11, 4039–4072, https://doi.org/10.5194/acp-11-4039-2011, 2011a.

Akagi, S. K., Craven, J. S., Taylor, J. W., McMeeking, G. R., Yokelson, R. J., Burling, I. R., Urbanski, S. P., Wold, C. E., Seinfeld, J. H., Coe, H., Alvarado, M. J., and Weise, D. R.: Evolution of trace gases and particles emitted by a chaparral fire in California, Atmos. Chem. Phys., 12, 1397–1421, https://doi.org/10.5194/acp-12-1397-2012, 2012.

Akherati, A., He, Y., Coggon, M. M., Koss, A. R., Hodshire, A. L., Sekimoto, K., Warneke, C., de Gouw, J., Yee, L., Seinfeld, J. H., Onasch, T. B., Herndon, S. C., Knighton, W. B., Cappa, C. D., Kleeman, M. J., Lim, C. Y., Kroll,

J. H., Pierce, J. R., and Jathar, S. H.: Oxygenated Aromatic Compounds are Important Precursors of Secondary Organic Aerosol in Biomass-Burning Emissions, Environ. Sci. Technol., 54, 8568–8579, https://doi.org/10.1021/acs.est.0c01345, 2020.

Al Ali, F., Cœur, C., Houzel, N., Genevray, P., Cazier, F., Cuisset, A., Papadimitriou, V. C., Tomas, A., and Romanias, M. N.: Products and yields for the NO3 radical initiated atmospheric degradation of 2-methylfuran (2-MF, CH3–C4H3O), Atmos. Environ., 319, 120276, https://doi.org/10.1016/j.atmosenv.2023.120276, 2024.

Allani, A., Bedjanian, Y., Papanastasiou, D. K., and Romanias, M. N.: Reaction Rate Coefficient of OH Radicals with d_9-Butanol as a Function of Temperature, ACS Omega, 6, 18123–18134, https://doi.org/10.1021/acsomega.1c01942, 2021.

An, Z., Yin, R., Zhao, X., Li, X., Li, Y., Yuan, Y., Guo, J., Zhao, Y., Li, X., Li, D., Li, Y., Wang, D., Yan, C., He, K., Worsnop, D. R., Keutsch, F. N., and Jiang, J.: Molecular and seasonal characteristics of organic vapors in urban Beijing: insights from Vocus-PTR measurements, Atmos. Chem. Phys., 24, 13793–13810, https://doi.org/10.5194/acp-24-13793-2024, 2024.

Anderson, M. J.: A new method for non-parametric multivariate analysis of variance, Austral Ecol., 26, 32–46, https://doi.org/10.1111/j.1442-9993.2001.01070.pp.x, 2001.

Anderson, M. J.: Permutational Multivariate Analysis of Variance (<scp>PERMANOVA</scp>), https://doi.org/10.1002/9781118445112.stat07841, 2017.

Andreae, M. O.: Emission of trace gases and aerosols from biomass burning – an updated assessment, Atmos. Chem. Phys., 19, 8523–8546, https://doi.org/10.5194/acp-19-8523-2019, 2019.

Atkinson, R.: Atmospheric chemistry of VOCs and NOx, Atmos. Environ., 34, 2063–2101, 2000.

Barmet, P., Dommen, J., DeCarlo, P. F., Tritscher, T., Praplan, A. P., Platt, S. M., Prévôt, A. S. H., Donahue, N. M., and Baltensperger, U.: OH clock determination by proton transfer reaction mass spectrometry at an environmental chamber, Atmos. Meas. Tech., 5, 647–656, https://doi.org/10.5194/amt-5-647-2012, 2012.

Bhattu, D., Zotter, P., Zhou, J., Stefenelli, G., Klein, F., Bertrand, A., Temime-Roussel, B., Marchand, N., Slowik, J. G., Baltensperger, U., Prévôt, A. S. H., Nussbaumer, T., El Haddad, I., and Dommen, J.: Effect of Stove Technology and Combustion Conditions on Gas and Particulate Emissions from Residential Biomass Combustion, Environ. Sci. Technol., 53, 2209–2219, https://doi.org/10.1021/acs.est.8b05020, 2019.

Ten Brink, P., Zádor, J., Turányi, T., Wirtz, K., Pilling, M. J., Kroll, J. H., Smith, J. D., Che, D. L., Kessler, S. H., Worsnop, D. R., Wilson, K. R., Zimmermann, R., Atkinson J., R. and A., Ng, N. L., Kroll, J. H., Chan, A. W. H., Chhabra, P. S., Flagan, R. C., Seinfeld, J. H., Kiendler-Scharr, A., Mensah, A. A., Friese, E., Topping, D., Nemitz, E., Prevot, A. S. H., Äijälä, M., Allan, J., Canonaco, F., Canagaratna, M. R., Carbone, S., Crippa, M., Dall Osto, M., Day, D. A., De Carlo, P., Di Marco, C. F., Elbern, H., Eriksson, A. C., Freney, E., Hao, L., Herrmann, H., Hildebrandt, L., Hillamo, R., Jimenez, J. L., Laaksonen, A., McFiggans, G., Mohr, C., O'Dowd, C., Otjes, R., Ovadnevaite, J., Pandis, S. N., Poulain, L., Schlag, P., Sellegri, K., Swietlicki, E., Tiitta, P., Vermeulen, A., Wahner, A., Worsnop, D. R., Wu, H. -C., Wong, K. W., Stutz, J., Moldoveanu, S., David, Victor., Henry, K. M., Donahue, N. M., Yunos, S. N. M. M., Ghafir, M. F. A., Wahab, A. A., He, Z., Zhang, Y. Y. Y., Yu, L., Liu, G., Zhou, D., Qian, Y., Lu, X., Mellouki, A., Wallington, T. J., Chen, J., He, Y., Zhao, B. B., Wang, S., Valorso, R., Chang, X., Yin, D., Feng, B., Camredon, M., Aumont, B., Dearden, A., Jathar, S. H., Shrivastava, M. K., Jiang, Z., Cappa, C. D., Yee, L. D., Seinfeld, J. H., Hao, J., Donahue, N. M., Löndahl, J., Möller, W., Pagels, J. H., et al.: Essentials in modern HPLC separations, Atmos. Chem. Phys., 11, 143686, https://doi.org/10.1016/j.proci.2004.08.276, 2022.

Brito, J., Rizzo, L. V., Morgan, W. T., Coe, H., Johnson, B., Haywood, J., Longo, K., Freitas, S., Andreae, M. O., and Artaxo, P.: Ground-based aerosol characterization during the South American Biomass Burning Analysis (SAMBBA) field experiment, Atmos. Chem. Phys., 14, 12069–12083, https://doi.org/10.5194/acp-14-12069-2014, 2014.

Bruns, E. A., El Haddad, I., Slowik, J. G., Kilic, D., Klein, F., Baltensperger, U., and Prévôt, A. S. H.: Identification of significant precursor gases of secondary organic aerosols from residential wood combustion, Sci. Rep., 6, 27881, https://doi.org/10.1038/srep27881, 2016.

Bruns, E. A., Slowik, J. G., El Haddad, I., Kilic, D., Klein, F., Dommen, J., Temime-Roussel, B., Marchand, N., Baltensperger, U., and Prévôt, A. S. H.: Characterization of gas-phase organics using proton transfer reaction time-of-flight mass spectrometry: fresh and aged residential wood combustion emissions, Atmos. Chem. Phys., 17, 705–720, https://doi.org/10.5194/acp-17-705-2017, 2017.

Calì Quaglia, F., Meloni, D., Muscari, G., Di Iorio, T., Ciardini, V., Pace, G., Becagli, S., Di Bernardino, A., Cacciani, M., Hannigan, J. W., Ortega, I., and di Sarra, A. G.: On the Radiative Impact of Biomass-Burning Aerosols in the Arctic: The August 2017 Case Study, Remote Sens. (Basel)., 14, 313, https://doi.org/10.3390/rs14020313, 2022.

Calvert, J. G., Atkinson, R., Becker, K. H., Kamens, R. M., Seinfeld, J. H., Wallington, T. J., and Yarwood, G.: The Mechanisms Of Atmospheric Oxidation Of Aromatic Hydrocarbons, Oxford University PressNew York, NY, https://doi.org/10.1093/oso/9780195146288.001.0001, 2002.

Chen, L.-W. A., Verburg, P., Shackelford, A., Zhu, D., Susfalk, R., Chow, J. C., and Watson, J. G.: Moisture effects on carbon and nitrogen emission from burning of wildland biomass, Atmos. Chem. Phys., 10, 6617–6625, https://doi.org/10.5194/acp-10-6617-2010, 2010.

Cheung, R. K. Y., Zhang, J., Wang, T., Kattner, L., Bogler, S., Puthussery, J. V., Huang, R.-J., Gysel-Beer, M., Slowik, J. G., Verma, V., Prevot, A. S. H., El Haddad, I., Bell, D. M., and Modini, R. L.: Online Measurements during Simulated Atmospheric Aging Track the Strongly Increasing Oxidative Potential of Complex Combustion Aerosols Relative to Their Primary Emissions, Environ. Sci. Technol. Lett., 12, 64–72, https://doi.org/10.1021/acs.estlett.4c00956, 2025.

Christian, T. J., Kleiss, B., Yokelson, R. J., Holzinger, R., Crutzen, P. J., Hao, W. M., Saharjo, B. H., and Ward, D. E.: Comprehensive laboratory measurements of biomass-burning emissions: 1. Emissions from Indonesian, African, and other fuels, Journal of Geophysical Research: Atmospheres, 108, https://doi.org/10.1029/2003JD003704, 2003.

Coggon, M. M., Lim, C. Y., Koss, A. R., Sekimoto, K., Yuan, B., Gilman, J. B., Hagan, D. H., Selimovic, V., Zarzana, K. J., Brown, S. S., Roberts, J. M., Müller, M., Yokelson, R., Wisthaler, A., Krechmer, J. E., Jimenez, J. L., Cappa, C., Kroll, J. H., de Gouw, J., and Warneke, C.: OH chemistry of non-methane organic gases (NMOGs) emitted from laboratory and ambient biomass burning smoke: evaluating the influence of furans and oxygenated aromatics on ozone and secondary NMOG formation, Atmos. Chem. Phys., 19, 14875–14899, https://doi.org/10.5194/acp-19-14875-2019, 2019.

Colmenar, I., González, S., Jiménez, E., Martín, P., Salgado, S., Cabañas, B., and Albaladejo, J.: UV absorption cross sections between 290 and 380 nm of a series of furanaldehydes: Estimation of their photolysis lifetimes, Atmos. Environ., 103, 1–6, https://doi.org/10.1016/j.atmosenv.2014.12.022, 2015.

Czech, H., Pieber, S. M., Tiitta, P., Sippula, O., Kortelainen, M., Lamberg, H., Grigonyte, J., Streibel, T., Prévôt, A. S. H., Jokiniemi, J., and Zimmermann, R.: Time-resolved analysis of primary volatile emissions and secondary aerosol formation potential from a small-scale pellet boiler, Atmos. Environ., 158, 236–245, https://doi.org/10.1016/j.atmosenv.2017.03.040, 2017.

Czech, H., Popovicheva, O., Chernov, D. G., Kozlov, A., Schneider, E., Shmargunov, V. P., Sueur, M., Rüger, C. P., Afonso, C., Uzhegov, V., Kozlov, V. S., Panchenko, M. V., and Zimmermann, R.: Wildfire plume ageing in the Photochemical Large Aerosol Chamber (PHOTO-LAC), Environ. Sci. Process. Impacts, 26, 35–55, https://doi.org/10.1039/D3EM00280B, 2024.

Dai, J., Zhang, K., Feng, Y., Yi, X., Li, R., Xue, J., Li, Q., Shi, L., Liao, J., Yi, Y., Wang, F., Yang, L., Chen, H., Huang, L., Tan, J., Wang, Y., and Li, L.: Significant influence of oxygenated volatile organic compounds on atmospheric chemistry: a case study in a typical industrial city in China, Atmos. Chem. Phys., 25, 7467–7484, https://doi.org/10.5194/acp-25-7467-2025, 2025.

Decker, Z. C. J., Robinson, M. A., Barsanti, K. C., Bourgeois, I., Coggon, M. M., DiGangi, J. P., Diskin, G. S., Flocke, F. M., Franchin, A., Fredrickson, C. D., Gkatzelis, G. I., Hall, S. R., Halliday, H., Holmes, C. D., Huey, L. G., Lee, Y. R., Lindaas, J., Middlebrook, A. M., Montzka, D. D., Moore, R., Neuman, J. A., Nowak, J. B., Palm, B. B., Peischl, J., Piel, F., Rickly, P. S., Rollins, A. W., Ryerson, T. B., Schwantes, R. H., Sekimoto, K., Thornhill, L., Thornton, J. A., Tyndall, G. S., Ullmann, K., Van Rooy, P., Veres, P. R., Warneke, C., Washenfelder, R. A., Weinheimer, A. J., Wiggins, E., Winstead, E., Wisthaler, A., Womack, C., and Brown, S. S.: Nighttime and daytime

dark oxidation chemistry in wildfire plumes: an observation and model analysis of FIREX-AQ aircraft data, Atmos. Chem. Phys., 21, 16293–16317, https://doi.org/10.5194/acp-21-16293-2021, 2021.

Dilger, M., Armant, O., Ramme, L., Mülhopt, S., Sapcariu, S. C., Schlager, C., Dilger, E., Reda, A., Orasche, J., Schnelle-Kreis, J., Conlon, T. M., Yildirim, A. Ö., Hartwig, A., Zimmermann, R., Hiller, K., Diabaté, S., Paur, H.-R., and Weiss, C.: Systems toxicology of complex wood combustion aerosol reveals gaseous carbonyl compounds as critical constituents, Environ. Int., 179, 108169, https://doi.org/10.1016/j.envint.2023.108169, 2023.

EU-JRC: Wildfires in the EU: 2022 was the second-worst year, a warning from a changing climate, 2023.

Fang, Z., Li, C., He, Q., Czech, H., Gröger, T., Zeng, J., Fang, H., Xiao, S., Pardo, M., Hartner, E., Meidan, D., Wang, X., Zimmermann, R., Laskin, A., and Rudich, Y.: Secondary organic aerosols produced from photochemical oxidation of secondarily evaporated biomass burning organic gases: Chemical composition, toxicity, optical properties, and climate effect, Environ. Int., 157, 106801, https://doi.org/10.1016/j.envint.2021.106801, 2021.

Fu, Y., Li, W., Manheim, J. M., Milton, J., Kilaz, G., and Kenttämaa, H. I.: Proton Affinities of Alkanes, J. Am. Soc. Mass Spectrom., 33, 1850–1857, https://doi.org/10.1021/jasms.2c00152, 2022.

Garofalo, L. A., Pothier, M. A., Levin, E. J. T., Campos, T., Kreidenweis, S. M., and Farmer, D. K.: Emission and Evolution of Submicron Organic Aerosol in Smoke from Wildfires in the Western United States, ACS Earth Space Chem., 3, 1237–1247, https://doi.org/10.1021/acsearthspacechem.9b00125, 2019.

Gehm, C., Schnepel, K., Czech, H., Miersch, T., Ehlert, S., and Zimmermann, R.: Hyper-fast gas chromatography and single-photon ionisation time-of-flight mass spectrometry with integrated electrical modulator-based sampling for headspace and online VOC analyses, Analyst, 146, 3137–3149, https://doi.org/10.1039/D1AN00114K, 2021.

Georgopoulou, M. P., Florou, K., Matrali, A., Starida, G., Kaltsonoudis, C., Nenes, A., and Pandis, S. N.: Diurnal aging of biomass burning emissions: impacts on secondary organic aerosol formation and oxidative potential, Atmos. Chem. Phys., 25, 15835–15855, https://doi.org/10.5194/acp-25-15835-2025, 2025.

Gilman, J. B., Lerner, B. M., Kuster, W. C., Goldan, P. D., Warneke, C., Veres, P. R., Roberts, J. M., de Gouw, J. A., Burling, I. R., and Yokelson, R. J.: Biomass burning emissions and potential air quality impacts of volatile organic compounds and other trace gases from fuels common in the US, Atmos. Chem. Phys., 15, 13915–13938, https://doi.org/10.5194/acp-15-13915-2015, 2015.

Gkatzelis, G. I., Coggon, M. M., Stockwell, C. E., Hornbrook, R. S., Allen, H., Apel, E. C., Bela, M. M., Blake, D. R., Bourgeois, I., Brown, S. S., Campuzano-Jost, P., St. Clair, J. M., Crawford, J. H., Crounse, J. D., Day, D. A., DiGangi, J. P., Diskin, G. S., Fried, A., Gilman, J. B., Guo, H., Hair, J. W., Halliday, H. S., Hanisco, T. F., Hannun, R., Hills, A., Huey, L. G., Jimenez, J. L., Katich, J. M., Lamplugh, A., Lee, Y. R., Liao, J., Lindaas, J., McKeen, S. A., Mikoviny, T., Nault, B. A., Neuman, J. A., Nowak, J. B., Pagonis, D., Peischl, J., Perring, A. E., Piel, F., Rickly, P. S., Robinson, M. A., Rollins, A. W., Ryerson, T. B., Schueneman, M. K., Schwantes, R. H., Schwarz, J. P., Sekimoto, K., Selimovic, V., Shingler, T., Tanner, D. J., Tomsche, L., Vasquez, K. T., Veres, P. R., Washenfelder, R., Weibring, P., Wennberg, P. O., Wisthaler, A., Wolfe, G. M., Womack, C. C., Xu, L., Ball, K., Yokelson, R. J., and Warneke, C.: Parameterizations of US wildfire and prescribed fire emission ratios and emission factors based on FIREX-AQ aircraft measurements, Atmos. Chem. Phys., 24, 929–956, https://doi.org/10.5194/acp-24-929-2024, 2024.

Gueneron, M., Erickson, M. H., VanderSchelden, G. S., and Jobson, B. T.: PTR-MS fragmentation patterns of gasoline hydrocarbons, Int. J. Mass Spectrom., 379, 97–109, https://doi.org/10.1016/j.ijms.2015.01.001, 2015.

Han, J., Wang, S., Yeung, K., Yang, D., Gu, W., Ma, Z., Sun, J., Wang, X., Chow, C.-W., Chan, A. W. H., and Peng, H.: Proteome-wide effects of naphthalene-derived secondary organic aerosol in BEAS-2B cells are caused by short-lived unsaturated carbonyls, Proceedings of the National Academy of Sciences, 117, 25386–25395, https://doi.org/10.1073/pnas.2001378117, 2020.

Hansel, A., Jordan, A., Holzinger, R., Prazeller, P., Vogel, W., and Lindinger, W.: Proton transfer reaction mass spectrometry: on-line trace gas analysis at the ppb level, Int. J. Mass Spectrom. Ion Process., 149–150, 609–619, https://doi.org/10.1016/0168-1176(95)04294-U, 1995.

Hartikainen, A., Yli-Pirilä, P., Tiitta, P., Leskinen, A., Kortelainen, M., Orasche, J., Schnelle-Kreis, J., Lehtinen, K. E. J., Zimmermann, R., Jokiniemi, J., and Sippula, O.: Volatile Organic Compounds from Logwood Combustion: Emissions and Transformation under Dark and Photochemical Aging Conditions in a Smog Chamber, Environ. Sci. Technol., 52, 4979–4988, https://doi.org/10.1021/acs.est.7b06269, 2018.

Hartikainen, A. H., Basnet, S., Yli-Pirilä, P., Ihalainen, M., Talvinen, S., Tissari, J., Mikkonen, S., Zimmermann, R., and Sippula, O.: Resolving emission factors and formation pathways of organic gaseous compounds from residential combustion of European brown coal, Combust. Flame, 265, 113485, https://doi.org/10.1016/j.combustflame.2024.113485, 2024.

Hatch, L. E., Yokelson, R. J., Stockwell, C. E., Veres, P. R., Simpson, I. J., Blake, D. R., Orlando, J. J., and Barsanti, K. C.: Multi-instrument comparison and compilation of non-methane organic gas emissions from biomass burning and implications for smoke-derived secondary organic aerosol precursors, Atmos. Chem. Phys., 17, 1471–1489, https://doi.org/10.5194/acp-17-1471-2017, 2017.

Hayden, K. L., Li, S.-M., Liggio, J., Wheeler, M. J., Wentzell, J. J. B., Leithead, A., Brickell, P., Mittermeier, R. L., Oldham, Z., Mihele, C. M., Staebler, R. M., Moussa, S. G., Darlington, A., Wolde, M., Thompson, D., Chen, J., Griffin, D., Eckert, E., Ditto, J. C., He, M., and Gentner, D. R.: Reconciling the total carbon budget for boreal forest wildfire emissions using airborne observations, Atmos. Chem. Phys., 22, 12493–12523, https://doi.org/10.5194/acp-22-12493-2022, 2022.

He, Y., Zhao, B., Wang, S., Valorso, R., Chang, X., Yin, D., Feng, B., Camredon, M., Aumont, B., Dearden, A., Jathar, S. H., Shrivastava, M., Jiang, Z., Cappa, C. D., Yee, L. D., Seinfeld, J. H., Hao, J., and Donahue, N. M.: Formation of secondary organic aerosol from wildfire emissions enhanced by long-time ageing, Nat. Geosci., 17, 124–129, https://doi.org/10.1038/s41561-023-01355-4, 2024.

Henze, D. K., Seinfeld, J. H., Ng, N. L., Kroll, J. H., Fu, T.-M., Jacob, D. J., and Heald, C. L.: Global modeling of secondary organic aerosol formation from aromatic hydrocarbons: high- vs. low-yield pathways, Atmos. Chem. Phys., 8, 2405–2420, https://doi.org/10.5194/acp-8-2405-2008, 2008.

Hobbs, P. V., Sinha, P., Yokelson, R. J., Christian, T. J., Blake, D. R., Gao, S., Kirchstetter, T. W., Novakov, T., and Pilewskie, P.: Evolution of gases and particles from a savanna fire in South Africa, Journal of Geophysical Research: Atmospheres, 108, https://doi.org/10.1029/2002JD002352, 2003.

Hodshire, A. L., Akherati, A., Alvarado, M. J., Brown-Steiner, B., Jathar, S. H., Jimenez, J. L., Kreidenweis, S. M., Lonsdale, C. R., Onasch, T. B., Ortega, A. M., and Pierce, J. R.: Aging Effects on Biomass Burning Aerosol Mass and Composition: A Critical Review of Field and Laboratory Studies, Environ. Sci. Technol., 53, 10007–10022, https://doi.org/10.1021/acs.est.9b02588, 2019.

Jaars, K., van Zyl, P. G., Beukes, J. P., Hellén, H., Vakkari, V., Josipovic, M., Venter, A. D., Räsänen, M., Knoetze, L., Cilliers, D. P., Siebert, S. J., Kulmala, M., Rinne, J., Guenther, A., Laakso, L., and Hakola, H.: Measurements of biogenic volatile organic compounds at a grazed savannah grassland agricultural landscape in South Africa, Atmos. Chem. Phys., 16, 15665–15688, https://doi.org/10.5194/acp-16-15665-2016, 2016.

Jaffe, D. A. and Wigder, N. L.: Ozone production from wildfires: A critical review, Atmos. Environ., 51, 1–10, https://doi.org/10.1016/j.atmosenv.2011.11.063, 2012.

Jen, C. N., Hatch, L. E., Selimovic, V., Yokelson, R. J., Weber, R., Fernandez, A. E., Kreisberg, N. M., Barsanti, K. C., and Goldstein, A. H.: Speciated and total emission factors of particulate organics from burning western US wildland fuels and their dependence on combustion efficiency, Atmos. Chem. Phys., 19, 1013–1026, https://doi.org/10.5194/acp-19-1013-2019, 2019.

Jensen, A. R., Koss, A. R., Hales, R. B., and de Gouw, J. A.: Measurements of volatile organic compounds in ambient air by gas-chromatography and real-time Vocus PTR-TOF-MS: calibrations, instrument background corrections, and introducing a PTR Data Toolkit, Atmos. Meas. Tech., 16, 5261–5285, https://doi.org/10.5194/amt-16-5261-2023, 2023.

Jin, L., Coggon, M. M., Permar, W., Juncosa Calahorrano, J. F., Palm, B. B., Gkatzelis, G. I., Robinson, M. A., Bourgeois, I., Hall, S. R., Peischl, J., Ullmann, K., Thornton, J. A., Warneke, C., Flocke, F., Fischer, E. V.,

Yokelson, R. J., and Hu, L.: Ozone photochemistry in fresh biomass burning smoke over the United States, Sci. Adv., 12, https://doi.org/10.1126/sciadv.ads2157, 2026.

Junninen, H., Ehn, M., Petäjä, T., Luosujärvi, L., Kotiaho, T., Kostiainen, R., Rohner, U., Gonin, M., Fuhrer, K., Kulmala, M., and Worsnop, D. R.: A high-resolution mass spectrometer to measure atmospheric ion composition, Atmos. Meas. Tech., 3, 1039–1053, https://doi.org/10.5194/amt-3-1039-2010, 2010.

Kawamura, K., Okuzawa, K., Aggarwal, S. G., Irie, H., Kanaya, Y., and Wang, Z.: Determination of gaseous and particulate carbonyls (glycolaldehyde, hydroxyacetone, glyoxal, methylglyoxal, nonanal and decanal) in the atmosphere at Mt. Tai, Atmos. Chem. Phys., 13, 5369–5380, https://doi.org/10.5194/acp-13-5369-2013, 2013.

Keywood, M., Kanakidou, M., Stohl, A., Dentener, F., Grassi, G., Meyer, C. P., Torseth, K., Edwards, D., Thompson, A. M., Lohmann, U., and Burrows, J.: Fire in the Air: Biomass Burning Impacts in a Changing Climate, Crit. Rev. Environ. Sci. Technol., 43, 40–83, https://doi.org/10.1080/10643389.2011.604248, 2013.

Kodros, J. K., Papanastasiou, D. K., Paglione, M., Masiol, M., Squizzato, S., Florou, K., Skyllakou, K., Kaltsonoudis, C., Nenes, A., and Pandis, S. N.: Rapid dark aging of biomass burning as an overlooked source of oxidized organic aerosol, Proceedings of the National Academy of Sciences, 117, 33028–33033, https://doi.org/10.1073/pnas.2010365117, 2020.

Kodros, J. K., Kaltsonoudis, C., Paglione, M., Florou, K., Jorga, S., Vasilakopoulou, C., Cirtog, M., Cazaunau, M., Picquet-Varrault, B., Nenes, A., and Pandis, S. N.: Secondary aerosol formation during the dark oxidation of residential biomass burning emissions, Environmental Science: Atmospheres, 2, 1221–1236, https://doi.org/10.1039/D2EA00031H, 2022.

Kolden, C. A., Abatzoglou, J. T., Jones, M. W., and Jain, P.: Wildfires in 2023, Nat. Rev. Earth Environ., 5, 238–240, https://doi.org/10.1038/s43017-024-00544-y, 2024.

Koss, A. R., Sekimoto, K., Gilman, J. B., Selimovic, V., Coggon, M. M., Zarzana, K. J., Yuan, B., Lerner, B. M., Brown, S. S., Jimenez, J. L., Krechmer, J., Roberts, J. M., Warneke, C., Yokelson, R. J., and de Gouw, J.: Non-methane organic gas emissions from biomass burning: identification, quantification, and emission factors from PTR-ToF during the FIREX 2016 laboratory experiment, Atmos. Chem. Phys., 18, 3299–3319, https://doi.org/10.5194/acp-18-3299-2018, 2018.

Köster, K., Kohli, J., Lindberg, H., and Pumpanen, J.: Post-fire soil greenhouse gas fluxes in boreal Scots pine forests–Are they affected by surface fires with different severities?, Agric. For. Meteorol., 349, 109954, https://doi.org/10.1016/j.agrformet.2024.109954, 2024.

Krechmer, J., Lopez-Hilfiker, F., Koss, A., Hutterli, M., Stoermer, C., Deming, B., Kimmel, J., Warneke, C., Holzinger, R., Jayne, J., Worsnop, D., Fuhrer, K., Gonin, M., and de Gouw, J.: Evaluation of a New Reagent-Ion Source and Focusing Ion–Molecule Reactor for Use in Proton-Transfer-Reaction Mass Spectrometry, Anal. Chem., 90, 12011–12018, https://doi.org/10.1021/acs.analchem.8b02641, 2018.

Kroll, J. H. and Seinfeld, J. H.: Chemistry of secondary organic aerosol: Formation and evolution of low-volatility organics in the atmosphere, Atmos. Environ., 42, 3593–3624, https://doi.org/10.1016/j.atmosenv.2008.01.003, 2008.

Kroll, J. H., Smith, J. D., Che, D. L., Kessler, S. H., Worsnop, D. R., and Wilson, K. R.: Measurement of fragmentation and functionalization pathways in the heterogeneous oxidation of oxidized organic aerosol, Physical Chemistry Chemical Physics, 11, 8005, https://doi.org/10.1039/b905289e, 2009.

Lambe, A. T., Onasch, T. B., Croasdale, D. R., Wright, J. P., Martin, A. T., Franklin, J. P., Massoli, P., Kroll, J. H., Canagaratna, M. R., Brune, W. H., Worsnop, D. R., and Davidovits, P.: Transitions from Functionalization to Fragmentation Reactions of Laboratory Secondary Organic Aerosol (SOA) Generated from the OH Oxidation of Alkane Precursors, Environ. Sci. Technol., 46, 5430–5437, https://doi.org/10.1021/es300274t, 2012.

Leskinen, A., Yli-Pirilä, P., Kuuspalo, K., Sippula, O., Jalava, P., Hirvonen, M.-R., Jokiniemi, J., Virtanen, A., Komppula, M., and Lehtinen, K. E. J.: Characterization and testing of a new environmental chamber, Atmos. Meas. Tech., 8, 2267–2278, https://doi.org/10.5194/amt-8-2267-2015, 2015.

Lewis, A. C., Carslaw, N., Marriott, P. J., Kinghorn, R. M., Morrison, P., Lee, A. L., Bartle, K. D., and Pilling, M. J.: A larger pool of ozone-forming carbon compounds in urban atmospheres, Nature, 405, 778–781, https://doi.org/10.1038/35015540, 2000.

Lewis, A. C., Evans, M. J., Hopkins, J. R., Punjabi, S., Read, K. A., Purvis, R. M., Andrews, S. J., Moller, S. J., Carpenter, L. J., Lee, J. D., Rickard, A. R., Palmer, P. I., and Parrington, M.: The influence of biomass burning on the global distribution of selected non-methane organic compounds, Atmos. Chem. Phys., 13, 851–867, https://doi.org/10.5194/acp-13-851-2013, 2013.

Li, H., Riva, M., Rantala, P., Heikkinen, L., Daellenbach, K., Krechmer, J. E., Flaud, P.-M., Worsnop, D., Kulmala, M., Villenave, E., Perraudin, E., Ehn, M., and Bianchi, F.: Terpenes and their oxidation products in the French Landes forest: insights from Vocus PTR-TOF measurements, Atmos. Chem. Phys., 20, 1941–1959, https://doi.org/10.5194/acp-20-1941-2020, 2020.

Li, H., Almeida, T. G., Luo, Y., Zhao, J., Palm, B. B., Daub, C. D., Huang, W., Mohr, C., Krechmer, J. E., Kurtén, T., and Ehn, M.: Fragmentation inside proton-transfer-reaction-based mass spectrometers limits the detection of ROOR and ROOH peroxides, Atmos. Meas. Tech., 15, 1811–1827, https://doi.org/10.5194/amt-15-1811-2022, 2022a.

Li, J., Xie, X., Li, L., Wang, X., Wang, H., Jing, S., Ying, Q., Qin, M., and Hu, J.: Fate of Oxygenated Volatile Organic Compounds in the Yangtze River Delta Region: Source Contributions and Impacts on the Atmospheric Oxidation Capacity, Environ. Sci. Technol., 56, 11212–11224, https://doi.org/10.1021/acs.est.2c00038, 2022b.

Li, K., Zhang, J., Bell, D. M., Wang, T., Lamkaddam, H., Cui, T., Qi, L., Surdu, M., Wang, D., Du, L., El Haddad, I., Slowik, J. G., and Prevot, A. S. H.: Uncovering the dominant contribution of intermediate volatility compounds in secondary organic aerosol formation from biomass-burning emissions, Natl. Sci. Rev., 11, https://doi.org/10.1093/nsr/nwae014, 2024a.

Li, R., Li, S., Jiang, X., Wu, Y., and Hu, K.: Organic Vapors from Residential Biomass Combustion: Emission Characteristics and Conversion to Secondary Organic Aerosols, Atmosphere (Basel)., 15, 692, https://doi.org/10.3390/atmos15060692, 2024b.

Li, S., Liu, D., Wu, Y., Hu, K., Jiang, X., Tian, P., Sheng, J., Pan, B., and Zhao, D.: Aging effects on residential biomass burning emissions under quasi-real atmospheric conditions, Environmental Pollution, 337, 122615, https://doi.org/10.1016/j.envpol.2023.122615, 2023.

Liang, C., Wang, S., Zhao, B., Xie, J., Li, Y., Feng, B., He, Y., Hou, S., Huang, L., Qu, Q., Zhang, H., Zhu, L., Jiang, J., and Hao, J.: Secondary Organic Aerosol Formation from the Photooxidation of Aromatic Ketone Intermediate Volatile Organic Compounds, Environ. Sci. Technol., 58, 21275–21285, https://doi.org/10.1021/acs.est.4c05384, 2024.

Liang, Y., Weber, R. J., Misztal, P. K., Jen, C. N., and Goldstein, A. H.: Aging of Volatile Organic Compounds in October 2017 Northern California Wildfire Plumes, Environ. Sci. Technol., 56, 1557–1567, https://doi.org/10.1021/acs.est.1c05684, 2022a.

Liang, Y., Stamatis, C., Fortner, E. C., Wernis, R. A., Van Rooy, P., Majluf, F., Yacovitch, T. I., Daube, C., Herndon, S. C., Kreisberg, N. M., Barsanti, K. C., and Goldstein, A. H.: Emissions of organic compounds from western US wildfires and their near-fire transformations, Atmos. Chem. Phys., 22, 9877–9893, https://doi.org/10.5194/acp-22-9877-2022, 2022b.

Liu, C., Chen, T., Liu, Y., Liu, J., He, H., and Zhang, P.: Enhancement of secondary organic aerosol formation and its oxidation state by SO_2 during photooxidation of 2-methoxyphenol, Atmos. Chem. Phys., 19, 2687–2700, https://doi.org/10.5194/acp-19-2687-2019, 2019.

Liu, Q., Gao, Y., Huang, W., Ling, Z., Wang, Z., and Wang, X.: Carbonyl compounds in the atmosphere: A review of abundance, source and their contributions to O3 and SOA formation, Atmos. Res., 274, 106184, https://doi.org/10.1016/j.atmosres.2022.106184, 2022.

Liu, T., Huang, D. D., Li, Z., Liu, Q., Chan, M., and Chan, C. K.: Comparison of secondary organic aerosol formation from toluene on initially wet and dry ammonium sulfate particles at moderate relative humidity, Atmos. Chem. Phys., 18, 5677–5689, https://doi.org/10.5194/acp-18-5677-2018, 2018.

Malecha, K. T. and Nizkorodov, S. A.: Photodegradation of Secondary Organic Aerosol Particles as a Source of Small, Oxygenated Volatile Organic Compounds, Environ. Sci. Technol., 50, 9990–9997, https://doi.org/10.1021/acs.est.6b02313, 2016.

Marques, M. M., Beland, F. A., Lachenmeier, D. W., Phillips, D. H., Chung, F.-L., Dorman, D. C., Elmore, S. E., Hammond, S. K., Krstev, S., Linhart, I., Long, A. S., Mandrioli, D., Ogawa, K., Pappas, J. J., Parra Morte, J. M., Talaska, G., Tang, M., Thakur, N., van Tongeren, M., Vineis, P., Grosse, Y., Benbrahim-Tallaa, L., Suonio, E., Turner, M. C., El Ghissassi, F., Middleton, D., Miranda-Filho, A., Chung, F., Liu, Y., Vega, S., Mattock, H., Schubauer-Berigan, M. K., and Guyton, K. Z.: Carcinogenicity of acrolein, crotonaldehyde, and arecoline, Lancet Oncol., 22, 19–20, https://doi.org/10.1016/S1470-2045(20)30727-0, 2021.

Mason, S. A., Field, R. J., Yokelson, R. J., Kochivar, M. A., Tinsley, M. R., Ward, D. E., and Hao, W. M.: Complex effects arising in smoke plume simulations due to inclusion of direct emissions of oxygenated organic species from biomass combustion, Journal of Geophysical Research: Atmospheres, 106, 12527–12539, https://doi.org/10.1029/2001JD900003, 2001.

McKeen, S. A., Wotawa, G., Parrish, D. D., Holloway, J. S., Buhr, M. P., Hübler, G., Fehsenfeld, F. C., and Meagher, J. F.: Ozone production from Canadian wildfires during June and July of 1995, Journal of Geophysical Research: Atmospheres, 107, https://doi.org/10.1029/2001JD000697, 2002.

Mukherjee, A., Hartikainen, A., Somero, M., Luostari, V., Ihalainen, M., Rüger, C. P., Kekäläinen, T., Nissinen, V. H., Barreira, L. M. F., Koponen, H., Kokkola, T., Li, D., Vettikkat, L., Yli-Pirilä, P., Shahzaib, M., Ruppel, M. M., Vakkari, V., Jaars, K., Siebert, S. J., Buchholz, A., Köster, K., van Zyl, P. G., Timonen, H., Kinnunen, N., Jänis, J., Virtanen, A., Virkkula, A., and Sippula, O.: Brown carbon emissions from laboratory combustion of Eurasian arctic-boreal and South African savanna biomass, Atmos. Chem. Phys., 25, 16747–16774, https://doi.org/10.5194/acp-25-16747-2025, 2025.

Müller, M., Anderson, B. E., Beyersdorf, A. J., Crawford, J. H., Diskin, G. S., Eichler, P., Fried, A., Keutsch, F. N., Mikoviny, T., Thornhill, K. L., Walega, J. G., Weinheimer, A. J., Yang, M., Yokelson, R. J., and Wisthaler, A.: In situ measurements and modeling of reactive trace gases in a small biomass burning plume, Atmos. Chem. Phys., 16, 3813–3824, https://doi.org/10.5194/acp-16-3813-2016, 2016.

Nguyen, D.-L., Czech, H., Pieber, S. M., Schnelle-Kreis, J., Steinbacher, M., Orasche, J., Henne, S., Popovicheva, O. B., Abbaszade, G., Engling, G., Bukowiecki, N., Nguyen, N.-A., Nguyen, X.-A., and Zimmermann, R.: Carbonaceous aerosol composition in air masses influenced by large-scale biomass burning: a case study in northwestern Vietnam, Atmos. Chem. Phys., 21, 8293–8312, https://doi.org/10.5194/acp-21-8293-2021, 2021.

Pagonis, D., Selimovic, V., Campuzano-Jost, P., Guo, H., Day, D. A., Schueneman, M. K., Nault, B. A., Coggon, M. M., DiGangi, J. P., Diskin, G. S., Fortner, E. C., Gargulinski, E. M., Gkatzelis, G. I., Hair, J. W., Herndon, S. C., Holmes, C. D., Katich, J. M., Nowak, J. B., Perring, A. E., Saide, P., Shingler, T. J., Soja, A. J., Thapa, L. H., Warneke, C., Wiggins, E. B., Wisthaler, A., Yacovitch, T. I., Yokelson, R. J., and Jimenez, J. L.: Impact of Biomass Burning Organic Aerosol Volatility on Smoke Concentrations Downwind of Fires, Environ. Sci. Technol., 57, 17011–17021, https://doi.org/10.1021/acs.est.3c05017, 2023.

Palm, B. B., Campuzano-Jost, P., Ortega, A. M., Day, D. A., Kaser, L., Jud, W., Karl, T., Hansel, A., Hunter, J. F., Cross, E. S., Kroll, J. H., Peng, Z., Brune, W. H., and Jimenez, J. L.: In situ secondary organic aerosol formation from ambient pine forest air using an oxidation flow reactor, Atmos. Chem. Phys., 16, 2943–2970, https://doi.org/10.5194/acp-16-2943-2016, 2016.

Palm, B. B., Peng, Q., Fredrickson, C. D., Lee, B. H., Garofalo, L. A., Pothier, M. A., Kreidenweis, S. M., Farmer, D. K., Pokhrel, R. P., Shen, Y., Murphy, S. M., Permar, W., Hu, L., Campos, T. L., Hall, S. R., Ullmann, K., Zhang, X., Flocke, F., Fischer, E. V., and Thornton, J. A.: Quantification of organic aerosol and brown carbon evolution in fresh wildfire plumes, Proceedings of the National Academy of Sciences, 117, 29469–29477, https://doi.org/10.1073/pnas.2012218117, 2020.

Pearson, R. K., Neuvo, Y., Astola, J., and Gabbouj, M.: Generalized Hampel Filters, EURASIP J. Adv. Signal Process., 2016, 87, https://doi.org/10.1186/s13634-016-0383-6, 2016.

Permar, W., Wang, Q., Selimovic, V., Wielgasz, C., Yokelson, R. J., Hornbrook, R. S., Hills, A. J., Apel, E. C., Ku, I., Zhou, Y., Sive, B. C., Sullivan, A. P., Collett, J. L., Campos, T. L., Palm, B. B., Peng, Q., Thornton, J. A., Garofalo, L. A., Farmer, D. K., Kreidenweis, S. M., Levin, E. J. T., DeMott, P. J., Flocke, F., Fischer, E. V., and Hu, L.: Emissions of Trace Organic Gases From Western U.S. Wildfires Based on WE-CAN Aircraft Measurements, Journal of Geophysical Research: Atmospheres, 126, https://doi.org/10.1029/2020JD033838, 2021.

Pfister, G. G., Wiedinmyer, C., and Emmons, L. K.: Impacts of the fall 2007 California wildfires on surface ozone: Integrating local observations with global model simulations, Geophys. Res. Lett., 35, https://doi.org/10.1029/2008GL034747, 2008.

Pospisilova, V., Lopez-Hilfiker, F. D., Bell, D. M., El Haddad, I., Mohr, C., Huang, W., Heikkinen, L., Xiao, M., Dommen, J., Prevot, A. S. H., Baltensperger, U., and Slowik, J. G.: On the fate of oxygenated organic molecules in atmospheric aerosol particles, Sci. Adv., 6, https://doi.org/10.1126/sciadv.aax8922, 2020.

Reinecke, T., Leiminger, M., Jordan, A., Wisthaler, A., and Müller, M.: Ultrahigh Sensitivity PTR-MS Instrument with a Well-Defined Ion Chemistry, Anal. Chem., 95, 11879–11884, https://doi.org/10.1021/acs.analchem.3c02669, 2023.

Rivera-Adorno, F. A., Tomlin, J. M., Lata, N. N., Azzarello, L., Robinson, M. A., Washenfelder, R. A., Franchin, A., Middlebrook, A. M., China, S., Brown, S. S., Young, C. J., Fraund, M., Moffet, R. C., and Laskin, A.: Chemical Imaging of Atmospheric Biomass Burning Particles from North American Wildfires, ACS ES&T Air, 2, 508–521, https://doi.org/10.1021/acsestair.4c00242, 2025.

Rogers, H. M., Ditto, J. C., and Gentner, D. R.: Evidence for impacts on surface-level air quality in the northeastern US from long-distance transport of smoke from North American fires during the Long Island Sound Tropospheric Ozone Study (LISTOS) 2018, Atmos. Chem. Phys., 20, 671–682, https://doi.org/10.5194/acp-20-671-2020, 2020.

Romanias, M. N., Coggon, M. M., Al Ali, F., Burkholder, J. B., Dagaut, P., Decker, Z., Warneke, C., Stockwell, C. E., Roberts, J. M., Tomas, A., Houzel, N., Coeur, C., and Brown, S. S.: Emissions and Atmospheric Chemistry of Furanoids from Biomass Burning: Insights from Laboratory to Atmospheric Observations, ACS Earth Space Chem., 8, 857–899, https://doi.org/10.1021/acsearthspacechem.3c00226, 2024.

San-Miguel-Ayanz Durrant, T., Boca, R., Maianti, P., Libertà, G., JACOME, F.O., Branco, A., DE, R., Suarez-Moreno, M., Ferrari, D. and Roglia, E., J.: Forest Fires in Europe, Middle East and North Africa 2022, Publications Office of the European Union, Luxembourg, 2023.

Sato, K., Hatakeyama, S., and Imamura, T.: Secondary Organic Aerosol Formation during the Photooxidation of Toluene: NO_x Dependence of Chemical Composition, J. Phys. Chem. A, 111, 9796–9808, https://doi.org/10.1021/jp071419f, 2007.

Schneider, E., Czech, H., Popovicheva, O., Chichaeva, M., Kobelev, V., Kasimov, N., Minkina, T., Rüger, C. P., and Zimmermann, R.: Mass spectrometric analysis of unprecedented high levels of carbonaceous aerosol particles long-range transported from wildfires in the Siberian Arctic, Atmos. Chem. Phys., 24, 553–576, https://doi.org/10.5194/acp-24-553-2024, 2024.

Sekimoto, K., Koss, A. R., Gilman, J. B., Selimovic, V., Coggon, M. M., Zarzana, K. J., Yuan, B., Lerner, B. M., Brown, S. S., Warneke, C., Yokelson, R. J., Roberts, J. M., and de Gouw, J.: High- and low-temperature pyrolysis profiles describe volatile organic compound emissions from western US wildfire fuels, Atmos. Chem. Phys., 18, 9263–9281, https://doi.org/10.5194/acp-18-9263-2018, 2018.

Shen, M., Ho, K. F., Dai, W., Liu, S., Zhang, T., Wang, Q., Meng, J., Chow, J. C., Watson, J. G., Cao, J., and Li, J.: Distribution and stable carbon isotopic composition of dicarboxylic acids, ketocarboxylic acids and α -dicarbonyls in fresh and aged biomass burning aerosols, Atmos. Chem. Phys., 22, 7489–7504, https://doi.org/10.5194/acp-22-7489-2022, 2022.

Simon, L., Gros, V., Petit, J.-E., Truong, F., Sarda-Estève, R., Kalalian, C., Baudic, A., Marchand, C., and Favez, O.: Two years of volatile organic compound online in situ measurements at the Site Instrumental de Recherche par

Télédétection Atmosphérique (Paris region, France) using proton-transfer-reaction mass spectrometry, Earth Syst. Sci. Data, 15, 1947–1968, https://doi.org/10.5194/essd-15-1947-2023, 2023.

Sinha, P., Hobbs, P. V., Yokelson, R. J., Bertschi, I. T., Blake, D. R., Simpson, I. J., Gao, S., Kirchstetter, T. W., and Novakov, T.: Emissions of trace gases and particles from savanna fires in southern Africa, Journal of Geophysical Research: Atmospheres, 108, https://doi.org/10.1029/2002JD002325, 2003.

Sokal, R. R. and Rohlf, F. J.: THE COMPARISON OF DENDROGRAMS BY OBJECTIVE METHODS, Taxon, 11, 33–40, https://doi.org/10.2307/1217208, 1962.

Stabbert, R., Dempsey, R., Diekmann, J., Euchenhofer, C., Hagemeister, T., Haussmann, H.-J., Knorr, A., Mueller, B. P., Pospisil, P., Reininghaus, W., Roemer, E., Tewes, F. J., and Veltel, D. J.: Studies on the contributions of smoke constituents, individually and in mixtures, in a range of in vitro bioactivity assays, Toxicology in Vitro, 42, 222–246, https://doi.org/10.1016/j.tiv.2017.04.003, 2017.

Stocker, M., Ladstädter, F., and Steiner, A. K.: Observing the climate impact of large wildfires on stratospheric temperature, Sci. Rep., 11, 22994, https://doi.org/10.1038/s41598-021-02335-7, 2021.

Stockwell, C. E., Veres, P. R., Williams, J., and Yokelson, R. J.: Characterization of biomass burning emissions from cooking fires, peat, crop residue, and other fuels with high-resolution proton-transfer-reaction time-of-flight mass spectrometry, Atmos. Chem. Phys., 15, 845–865, https://doi.org/10.5194/acp-15-845-2015, 2015.

Strollo, C. M. and Ziemann, P. J.: Products and mechanism of secondary organic aerosol formation from the reaction of 3-methylfuran with OH radicals in the presence of NOx, Atmos. Environ., 77, 534–543, https://doi.org/10.1016/j.atmosenv.2013.05.033, 2013.

Swap, R. J., Annegarn, H. J., Suttles, J. T., King, M. D., Platnick, S., Privette, J. L., and Scholes, R. J.: Africa burning: A thematic analysis of the Southern African Regional Science Initiative (SAFARI 2000), Journal of Geophysical Research: Atmospheres, 108, https://doi.org/10.1029/2003JD003747, 2003.

Tajuelo, M., Rodríguez, D., Rodríguez, A., Escalona, A., Viteri, G., Aranda, A., and Diaz-de-Mera, Y.: Secondary organic aerosol formation from the ozonolysis and oh-photooxidation of 2,5-dimethylfuran, Atmos. Environ., 245, 118041, https://doi.org/10.1016/j.atmosenv.2020.118041, 2021.

Tiitta, P., Leskinen, A., Hao, L., Yli-Pirilä, P., Kortelainen, M., Grigonyte, J., Tissari, J., Lamberg, H., Hartikainen, A., Kuuspalo, K., Kortelainen, A.-M., Virtanen, A., Lehtinen, K. E. J., Komppula, M., Pieber, S., Prévôt, A. S. H., Onasch, T. B., Worsnop, D. R., Czech, H., Zimmermann, R., Jokiniemi, J., and Sippula, O.: Transformation of logwood combustion emissions in a smog chamber: formation of secondary organic aerosol and changes in the primary organic aerosol upon daytime and nighttime aging, Atmos. Chem. Phys., 16, 13251–13269, https://doi.org/10.5194/acp-16-13251-2016, 2016.

Tkacik, D. S., Robinson, E. S., Ahern, A., Saleh, R., Stockwell, C., Veres, P., Simpson, I. J., Meinardi, S., Blake, D. R., Yokelson, R. J., Presto, A. A., Sullivan, R. C., Donahue, N. M., and Robinson, A. L.: A dual-chamber method for quantifying the effects of atmospheric perturbations on secondary organic aerosol formation from biomass burning emissions, Journal of Geophysical Research: Atmospheres, 122, 6043–6058, https://doi.org/10.1002/2016JD025784, 2017.

Travis, K. R., Crawford, James. H., Soja, A. J., Gargulinski, E. M., Moore, R. H., Wiggins, E. B., Diskin, G. S., DiGangi, J. P., Nowak, J. B., Halliday, H., Yokelson, R. J., McCarty, J. L., Simpson, I. J., Blake, D. R., Meinardi, S., Hornbrook, R. S., Apel, E. C., Hills, A. J., Warneke, C., Coggon, M. M., Rollins, A. W., Gilman, J. B., Womack, C. C., Robinson, M. A., Katich, J. M., Peischl, J., Gkatzelis, G. I., Bourgeois, I., Rickly, P. S., Lamplugh, A., Dibb, J. E., Jimenez, J. L., Campuzano-Jost, P., Day, D. A., Guo, H., Pagonis, D., Wennberg, P. O., Crounse, J. D., Xu, L., Hanisco, T. F., Wolfe, G. M., Liao, J., St. Clair, J. M., Nault, B. A., Fried, A., and Perring, A. E.: Emission Factors for Crop Residue and Prescribed Fires in the Eastern US During FIREX-AQ, Journal of Geophysical Research: Atmospheres, 128, https://doi.org/10.1029/2023JD039309, 2023a

Vakkari, V., Kerminen, V., Beukes, J. P., Tiitta, P., Zyl, P. G., Josipovic, M., Venter, A. D., Jaars, K., Worsnop, D. R., Kulmala, M., and Laakso, L.: Rapid changes in biomass burning aerosols by atmospheric oxidation, Geophys. Res. Lett., 41, 2644–2651, https://doi.org/10.1002/2014GL059396, 2014.

Vakkari, V., Beukes, J. P., Dal Maso, M., Aurela, M., Josipovic, M., and van Zyl, P. G.: Major secondary aerosol formation in southern African open biomass burning plumes, Nat. Geosci., 11, 580–583, https://doi.org/10.1038/s41561-018-0170-0, 2018.

Vakkari, V., Beukes, J. P., Josipovic, M., and van Zyl, P. G.: Observations of ozone formation in southern African savanna and grassland fire plumes, Atmos. Environ., 223, 117256, https://doi.org/10.1016/j.atmosenv.2019.117256, 2020.

Vakkari, V., Vettikkat, L., Kommula, S., Mukherjee, A., Hao, L., Backman, J., Buchholz, A., Gawlitta, N., Ihalainen, M., Jaars, K., Köster, K., Le, V., Miettinen, P., Nissinen, A., Czech, H., Alton, M., Passig, J., Peltokorpi, S., Piedehierro, A. A., Pullinen, I., Rosewig, E. I., Schobesberger, S., Shukla, D., Siebert, S. J., Somero, M., Virkkula, A., Welti, A., Yli-Pirilä, P., Ylisirniö, A., Zimmermann, R., van Zyl, P. G., Virtanen, A., and Sippula, O.: Laboratory Experiments on Savannah and European Boreal Forest Fire Emissions, Journal of Geophysical Research: Atmospheres, 131, https://doi.org/10.1029/2025JD044543, 2026.

Wang, T., Zhang, J., Lamkaddam, H., Li, K., Cheung, K. Y., Kattner, L., Gammelsæter, E., Bauer, M., Decker, Z. C. J., Bhattu, D., Huang, R., Modini, R. L., Slowik, J. G., El Haddad, I., Prevot, A. S. H., and Bell, D. M.: Chemical characterization of organic vapors from wood, straw, cow dung, and coal burning, Atmos. Chem. Phys., 25, 2707–2724, https://doi.org/10.5194/acp-25-2707-2025, 2025.

Ward, D. E. , & R. L. F.: Emissions measurements from vegetation fires: A comparative evaluation of methods and results. In P. J. Crutzen & J. G. Goldammer (Eds.), Fire in the environment: The ecological, atmospheric and climatic importance of vegetation fires, John Wiley, 53–76 pp., 1993.

Warneke, C., Schwarz, J. P., Dibb, J., Kalashnikova, O., Frost, G., Al-Saad, J., Brown, S. S., Brewer, Wm. A., Soja, A., Seidel, F. C., Washenfelder, R. A., Wiggins, E. B., Moore, R. H., Anderson, B. E., Jordan, C., Yacovitch, T. I., Herndon, S. C., Liu, S., Kuwayama, T., Jaffe, D., Johnston, N., Selimovic, V., Yokelson, R., Giles, D. M., Holben, B. N., Goloub, P., Popovici, I., Trainer, M., Kumar, A., Pierce, R. B., Fahey, D., Roberts, J., Gargulinski, E. M., Peterson, D. A., Ye, X., Thapa, L. H., Saide, P. E., Fite, C. H., Holmes, C. D., Wang, S., Coggon, M. M., Decker, Z. C. J., Stockwell, C. E., Xu, L., Gkatzelis, G., Aikin, K., Lefer, B., Kaspari, J., Griffin, D., Zeng, L., Weber, R., Hastings, M., Chai, J., Wolfe, G. M., Hanisco, T. F., Liao, J., Campuzano Jost, P., Guo, H., Jimenez, J. L., and Crawford, J.: Fire Influence on Regional to Global Environments and Air Quality (FIREX-AQ), Journal of Geophysical Research: Atmospheres, 128, https://doi.org/10.1029/2022JD037758, 2023.

Whitman, E., Parisien, M.-A., Thompson, D. K., and Flannigan, M. D.: Short-interval wildfire and drought overwhelm boreal forest resilience, Sci. Rep., 9, 18796, https://doi.org/10.1038/s41598-019-55036-7, 2019.

Wolfe, G. M., Hanisco, T. F., Arkinson, H. L., Blake, D. R., Wisthaler, A., Mikoviny, T., Ryerson, T. B., Pollack, I., Peischl, J., Wennberg, P. O., Crounse, J. D., St. Clair, J. M., Teng, A., Huey, L. G., Liu, X., Fried, A., Weibring, P., Richter, D., Walega, J., Hall, S. R., Ullmann, K., Jimenez, J. L., Campuzano-Jost, P., Bui, T. P., Diskin, G., Podolske, J. R., Sachse, G., and Cohen, R. C.: Photochemical evolution of the 2013 California Rim Fire: synergistic impacts of reactive hydrocarbons and enhanced oxidants, Atmos. Chem. Phys., 22, 4253–4275, https://doi.org/10.5194/acp-22-4253-2022, 2022.

Yazdani, A., Takahama, S., Kodros, J. K., Paglione, M., Masiol, M., Squizzato, S., Florou, K., Kaltsonoudis, C., Jorga, S. D., Pandis, S. N., and Nenes, A.: Chemical evolution of primary and secondary biomass burning aerosols during daytime and nighttime, Atmos. Chem. Phys., 23, 7461–7477, https://doi.org/10.5194/acp-23-7461-2023, 2023.

Yee, L. D., Kautzman, K. E., Loza, C. L., Schilling, K. A., Coggon, M. M., Chhabra, P. S., Chan, M. N., Chan, A. W. H., Hersey, S. P., Crounse, J. D., Wennberg, P. O., Flagan, R. C., and Seinfeld, J. H.: Secondary organic aerosol formation from biomass burning intermediates: phenol and methoxyphenols, Atmos. Chem. Phys., 13, 8019–8043, https://doi.org/10.5194/acp-13-8019-2013, 2013.

Yokelson, R. J., Goode, J. G., Ward, D. E., Susott, R. A., Babbitt, R. E., Wade, D. D., Bertschi, I., Griffith, D. W. T., and Hao, W. M.: Emissions of formaldehyde, acetic acid, methanol, and other trace gases from biomass fires in North Carolina measured by airborne Fourier transform infrared spectroscopy, Journal of Geophysical Research: Atmospheres, 104, 30109–30125, https://doi.org/10.1029/1999JD900817, 1999.

Yokelson, R. J., Christian, T. J., Karl, T. G., and Guenther, A.: The tropical forest and fire emissions experiment: laboratory fire measurements and synthesis of campaign data, Atmos. Chem. Phys., 8, 3509–3527, https://doi.org/10.5194/acp-8-3509-2008, 2008.

Yuan, B., Koss, A. R., Warneke, C., Coggon, M., Sekimoto, K., and de Gouw, J. A.: Proton-Transfer-Reaction Mass Spectrometry: Applications in Atmospheric Sciences, Chem. Rev., 117, 13187–13229, https://doi.org/10.1021/acs.chemrev.7b00325, 2017a.

Yuan, Y., Zhao, X., Wang, S., and Wang, L.: Atmospheric Oxidation of Furan and Methyl-Substituted Furans Initiated by Hydroxyl Radicals, J. Phys. Chem. A, 121, 9306–9319, https://doi.org/10.1021/acs.jpca.7b09741, 2017b.

Zhong, Q., Schutgens, N., Veraverbeke, S., and van der Werf, G. R.: Increasing aerosol emissions from boreal biomass burning exacerbate Arctic warming, Nat. Clim. Chang., 14, 1275–1281, https://doi.org/10.1038/s41558-024-02176-y, 2024.

Zhu, B., Huang, X.-F., Xia, S.-Y., Lin, L.-L., Cheng, Y., and He, L.-Y.: Biomass-burning emissions could significantly enhance the atmospheric oxidizing capacity in continental air pollution, Environmental Pollution, 285, 117523, https://doi.org/10.1016/j.envpol.2021.117523, 2021.

Ziemann, P. J. and Atkinson, R.: Kinetics, products, and mechanisms of secondary organic aerosol formation, Chem. Soc. Rev., 41, 6582, https://doi.org/10.1039/c2cs35122f, 2012.